Fall 1-31-2001

Analysis of discrete dynamical system models for competing species

Jerry J. Chen
New Jersey Institute of Technology

ABSTRACT

ANALYSIS OF DISCRETE DYNAMICAL SYSTEM MODELS FOR COMPETING SPECIES

by
Jerry J. Chen

A discrete version of the Lotka-Volterra (LV) differential equations for competing population species is analyzed in detail, much the same way as the discrete form of the logistic equation has been investigated as a source of bifurcation phenomena and chaotic dynamics. Another related system, namely, the Exponentially Self-Regulating (ESR) population model, is also thoroughly analyzed. It is found that in addition to logistic dynamics — ranging from the very simple to manifestly chaotic regimes in terms of the governing parameters — the discrete LV model and the ESR model exhibit their own brands of bifurcation and chaos that are essentially two-dimensional in nature. In particular, it is shown that both systems exhibit "twisted horseshoe" dynamics associated to a strange invariant set for certain parameter ranges.

ANALYSIS OF DISCRETE DYNAMICAL SYSTEM MODELS FOR COMPETING SPECIES

by
Jerry J. Chen

A Dissertation
Submitted to the Faculty of
New Jersey Institute of Technology
and Rutgers, The State University of New Jersey-Newark
in Partial Fulfillment of the Requirements for the Degree of
Doctor of Philosophy in Mathematical Sciences

Department of Mathematical Sciences
Department of Mathematics and Computer Science, Rutgers-Newark

January 2001

APPROVAL PAGE

ANALYSIS OF DISCRETE DYNAMICAL SYSTEM MODELS FOR COMPETING SPECIES

Jerry J. Chen

Dr. Denis Blackmore, Dissertation Advisor Professor of Mathematical Sciences, NJIT	Date
Dr. Amitabha Bose, Committee Member Assistant Professor of Mathematical Sciences, NJIT	Date
Dr. Victoria Booth, Committee Member Assistant Professor of Mathematical Sciences, NJIT	Date
Dr. Stanley Reisman, Committee Member Professor of Biomedical Engineering, NJIT Professor of Electrical and Computer Engineering, NJIT	Date
Dr. John Tavantzis, Committee Member Professor of Mathematical Sciences, NJIT	Date

BIOGRAPHICAL SKETCH

Author: Jerry J. Chen

Degree: Doctor of Philosophy

Date: January 2001

Undergraduate and Graduate Education:

- Doctor of Philosophy in Mathematical Sciences
  New Jersey Institute of Technology, Newark, NJ, January 2001

- Master of Science in Applied Mathematics
  New Jersey Institute of Technology, Newark, NJ, October 1996

- Bachelor of Science in Applied Mathematics
  New Jersey Institute of Technology, Newark, NJ, May 1995

Major: Mathematical Sciences

Publications:

D. Blackmore, J. Chen, J. Perez and M. Savescu,
"Dynamical Properties of Discrete Lotka-Volterra Equations,"
Chaos, Solitons and Fractals,
accepted for publication, September 2000.

D. Blackmore and J. Chen,
"On the Exponentially Self-Regulating Population Model,"
Journal of Mathematical Biology,
in preparation, January 2001.

D. Blackmore and J. Chen,
"Twisted Chaos in Discrete Population Models,"
Chaos, Solitons and Fractals,
in preparation, February 2001.

To my parents
and
I-Chih

ACKNOWLEDGMENT

First of all, I would like to give my greatest gratitude to Dr. Denis Blackmore, my advisor, for his guidance, patience and time. Without his continuous encouragement, I would not have made it this far in my graduate work. Then, I would thank the Department of Mathematical Sciences of NJIT for generous financial support of my graduate study from the beginning to the end. Thanks to Dr. John Tavantzis for the period of time when we investigated the Hénon map. Thank you also to Dr. Amitabha Bose, Dr. Demitri Papageorgiou and Dr. Stanley Reisman for serving as the members on my Ph.D. committee. A special thanks to Dr. Victoria Booth for agreeing to my last minute request to be the new committee member. Thanks also to my fellow graduate students in the program.

My parents are my faithful believers who are always there when I need them. Thank you, Mom and Dad. Without the endless support and love from I-Chih, this work would never have been accomplished. I deeply thank her. Last but not the least, thank you God.

TABLE OF CONTENTS

TABLE OF CONTENTS
(Continued)

Chapter **Page**

LIST OF TABLES

Table **Page**

LIST OF FIGURES

LIST OF FIGURES
(Continued)

Figure **Page**

CHAPTER 1
INTRODUCTION

In the past two decades, an increasing amount of attention has been addressed to the study of dynamical system models arising from biological systems. This is part of the development of a rich and diversified field that lies somewhere between mathematics and the sciences. Mathematical biology is one of the major branches of application in the study of the field of dynamical systems ([34]). The increasing use of mathematics in biology is inevitable as biological research becomes more dependent on quantitative analysis. The complexity of the biological sciences makes interdisciplinary involvement essential. The best designed models must show how a process works and then predict what may follow.

In the study of population biology, an accurate prediction of the evolution of quantities associated to any specific species is crucial and necessary ([22]). There are three principal types of interaction between two species, namely, prey-predator, competition and mutualism. It is known that in a prey-predator case, the growth rate of one species is reduced due to the existence of the other whereas in competition, the growth rates of both species are decreased while in mutualism, their growth rates are enhanced ([34]). Models may be used to explore the consequences of particular and restrictive assumptions which represent only part of the full picture ([52]). In fisheries biology, it is well-known that the simplest discrete-time population models have the potential for exhibiting bifurcations to periodic solutions with respect to parametric variation ([53] and [54]) or much more complicated behavior ([53] and [55]), and that there are serious concerns regarding the problem of parameter identification. Useful models should have dynamical behavior that is not too greatly affected by the small margin of error that is unavoidable in the measurement of environmental factors. From the biological point of view, a sound mathematical population model for the interaction of species should at least provide fairly accurate qualitative and

quantitative predictions concerning possible extinction of one or more species and long term (steady state) behavior of the species. There are, of course, several key biological parameters involved in the formulation of such models, ranging from the carrying capacity to the presence of the prey and predator. Typically, the dynamical evolution of the species (both qualitative and quantitative) varies significantly with these key parameters. To distinguish and categorize each possible type of dynamic behavior is the primary goal in studying population biology.

The logistic equation (map), as a population model for a single species obtained from a difference equation analog of the logistic differential equation on the line (see [9], [10], [13] and [14]), has come to be regarded as perhaps the simplest and best known paradigm of a dynamical system exhibiting an unexpectedly wide range of complicated phenomena ([1], [3], [5] and [8]). Its parameter-dependent dynamics have been extensively studied within the context of iterated one-dimensional maps and is now almost completely understood ([2]-[4], [6], [9], [11], [14] and [15]). In this report, an analogous discretization of the Lotka-Volterra differential equations in the plane for a pair of species in a population ([1], [7] and [10])is investigated along with an extensive, but by no means complete, analysis of the associated dynamics of the iterations. It shall be shown that the dynamics of the discrete Lotka-Volterra equations not only subsumes that of the one-dimensional logistic map, but also includes very complicated and quite new behavior that is intrinsically two-dimensional in nature. It is hoped that the results of the investigation will stimulate further study of the dynamics of the Lotka-Volterra map and related maps that appear to be useful for modeling the interaction of two or more species in a population.

As is well known ([1]), the motion of the logistic differential equation is simple and easy to analyze — which is in dramatic contrast with the discrete dynamics of the logistic map. The Lotka-Volterra differential equations in the plane also have

relatively simple dynamics in the phase plane ([1], [12] and [18]). For one thing, no chaotic motion is possible since the system is autonomous and two-dimensional, although it should be noted that chaotic regimes do occur in the three-dimensional version of these equations ([7]). One of the main purposes here is to demonstrate that the dynamical differences between the Lotka-Volterra differential equations and the Lotka-Volterra map in the plane are even more striking than in the logistic type.

The Hénon map ([5])is a two-parameter family of maps of the plane which possesses many of the dynamics and phenomena that we shall show occurring for the Lotka-Volterra map. Two obvious similarities are the horseshoe and the "strange repelling set". To simplify the LV map, the number of parameters can be reduced via topological conjugacies. It shall be shown that by examining a four-parameter family of maps, the full range of dynamics of the LV map, including chaotic regimes, can be characterized.

A horseshoe map is a simplified version of a map first studied by Smale ([17] and [51]), and, due to the shape of the image of the domain of the map, is called a *Smale horseshoe* ([42]). The LV map actually contains a new type of chaotic regime related to the Smale horseshoe for certain ranges of the key parameters. This horseshoe is orientation-reversing — exhibiting the standard stretching and folding of the horseshoe plus a twist. It appears that this twisted horseshoe behavior has not yet been described in the literature. There is a strange (Cantor-like) invariant set associated with the twisted horseshoe.

In this thesis, a related system, that we call the Exponentially Self-Regulating (ESR) population model, is studied in much the same way as the Lotka-Volterra model. The ESR model includes a self-regulating mechanism (such as cannibalism) that limits the sizes of the populations. It has been employed with considerable success in modeling actual populations and has been studied rather extensively ([49] and [50]). However, there are still many dynamical features of the ESR model that

are not completely understood. A careful analysis of the two-dimensional (competing pair of species in a population) ESR model dynamics is then undertaken together with numerical and statistical investigations. It is shown, for example, that the dynamics of the discrete ESR equations not only exhibit the same basic features as the two-dimensional LV map, but also includes very strange behavior that has not been observed before in discrete population models. This very unusual behavior corresponds to a strange attractor generated by twisted horseshoe dynamics. As with the analysis of the LV map, the investigation of the dynamics of the ESR model is accomplished by a combination of analytical and numerical techniques.

Although the dynamics of the discrete Lotka-Volterra, discrete Exponentially Self-Regulating and related models have been studied in the literature (see, eg. Nisbet and Onyiah [49], Costantino et al. [50], Franke and Yakubu [57-60] and Namkoong and Selgrade [61]), those studies have been restricted to the analysis of dynamics near fixed points, steady state phenomena and numerical simulation. Our work represents the first rigorous systematic study of the chaotic regimes that can arise in such models. In particular, we are apparently the first to identify and prove the existence of the twisted horseshoe regime. In our opinion, twisted horseshoe dynamics is the primary mechanism for chaotic dynamics and strange invariant sets — including strange attractors — in such low-dimensional competing species models. Unfortunately the data available in the literature on the evolution of real populations is not well-suited to making comparisons with predictions of the models we studied. The gathering of such data, preferably in collaboration with a population biologist, is a priority for our future research.

The dissertation is thereafter organized as follows: In Chapter 2, the first proposed model, the LV model, is formulated with all needed dynamical preliminaries followed by the analytical and numerical results. For the second proposed model, an analogous combination of analytical and numerical results will be described for the

ESR model in Chapter 3. Our analysis of both models is based on the modern theory of discrete dynamical systems while the numerical simulations are made using standard mathematical software such as Matlab. The dissertation concludes in Chapter 4 with a discussion of both analytical and numerical results obtained for the two models, a comparison of the dynamics of the two models, some concluding remarks, and the identification of some possible directions for future research.

CHAPTER 2

THE LOTKA-VOLTERRA MODEL

This chapter is organized as follows: In Section 2.1, we describe first the continuous form of the Lotka-Volterra dynamical system in the plane and then the associated discrete version (the Lotka-Volterra map) that is the subject of our investigation. Also, we discuss some normal forms of the planar Lotka-Volterra dynamical system that can be obtained using topological conjugacies (coordinate transformations). Next, in Section 2.2, we introduce some basic dynamical system notation for the Lotka-Volterra map. Then, we analyze several basic features of the map including the location and types of its fixed points in Section 2.3. We follow this in Section 2.4 with a brief description of a special uncoupled case of the Lotka-Volterra equations whose dynamics are essentially determined by those of the logistic map. In Section 2.5, we describe some aspects of the dynamics of a simple coupled quadratic case of the Lotka-Volterra equations. In Section 2.6, we prove that for certain ranges of the Lotka-Volterra map parameters, there is a chaotic regime generated by an orientation-reversing horseshoe map that we call a *twisted horseshoe.* Moreover, it is shown that the compact invariant set corresponding to the twisted horseshoe is essentially locally repelling — indicating that this population state is unstable.

2.1 The Lotka-Volterra Map

We start with the Lotka-Volterra system of differential equations in the plane which we take to be of the form ([1], [12] and [18])

$$\begin{aligned} \tfrac{dx}{dt} &= \lambda x(1 - ax - by) \quad \text{and} \\ \tfrac{dy}{dt} &= \mu y(1 - cx - dy) \end{aligned} \tag{2.1}$$

where the parameters λ and μ are both positive numbers and the parameters (or coefficients) are all nonnegative numbers and $a + b + c + d > 0$ in order to eliminate

the possibility of (2.1) being linear. In analogy with the association of the logistic map to the logistic differential equation, we define the (two-dimensional) Lotka-Volterra (LV) map to be the real analytic function $F : \mathbf{R}^2 \to \mathbf{R}^2$ defined by

$$F(x, y) := (\lambda x(1 - ax - by), \mu y(1 - cx - dy)), \tag{2.2}$$

where the six parameters are subject to the same conditions as in (2.1). Note that F depends on the parameters $\Pi := (\lambda, \mu, a, b, c, d)$ and should therefore perhaps be denoted by F_Π; in some cases in the sequel we shall explicitly denote this parameter dependence, but in most cases we shall simply maintain this slight and essentially harmless abuse of notation.

In certain cases the LV map can be recast in simpler (normal) forms that actually reduce the number of parameters. For example, when both a and d are positive, (2.2) is topologically conjugate to

$$F_0(x, y) := (\lambda x(1 - x - \alpha y), \mu y(1 - \beta x - y)), \tag{2.3}$$

with $\lambda, \mu > 0$ and $\alpha, \beta \geq 0$ via the conjugacy $\varphi : \mathbf{R}^2 \to \mathbf{R}^2$ defined by

$$\varphi(x, y) := (ax, dy).$$

On the other hand, with $\lambda, \mu > 0$, if $a = d = 0$ and $b, c > 0$, (2.2) is conjugate to

$$F_1(x, y) := (\lambda x(1 - y), \mu y(1 - x)) \tag{2.4}$$

via the topological conjugacy $\varphi(x, y) := (cx, by)$. We remark here that we have made obvious definitions or re-definitions of the parameters in the above normal forms. There are clearly other normal forms for other parameter choices, but we shall not consider them in the sequel. In particular, we shall investigate only (2.3) and (2.4), with comparatively little space being devoted to (2.4).

2.2 Dynamical Preliminaries

In what follows, we shall assume that the reader is familiar with the basic concepts of smooth discrete dynamical systems such as are to be found in [1, 5, 8, 16 and 17]. Nevertheless, a few preliminary remarks are in order since the iterations of F (under composition of functions) do not quite satisfy the requirements of such dynamical systems. The smooth (actually analytic) semigroup action $\mathbf{Z}_+ \times \mathbf{R}^2 \to \mathbf{R}^2$ defined by

$$(n, X) \mapsto F^n(X),$$

does constitute a smooth semidynamical system on $\mathbf{R}^2$, where $\mathbf{Z}_+$ is the additive semigroup of nonnegative integers, $\mathbf{R}^2 := \{(x, y) : x, y \in \mathbf{R}\}$ is the Euclidean plane, F^n is the n-fold composition of F with itself and $X := (x, y)$ is a point in $\mathbf{R}^2$ which will be treated as a row or column vector whenever contextually appropriate.

As the inverse of the LV map, F^{-1} is not globally defined, and not even locally definable at singular points of F. There is of course no canonical way to extend the above semigroup action to a group action of the integers $\mathbf{Z}$ on $\mathbf{R}^2$. The crux of the problem is that the inverse (relation) F^{-1} of F is a multivalued function such that it has four values almost everywhere (in the sense of Lebesgue measure on $\mathbf{R}^2$) on the image of F, but may have as few as one value or as many as a continuum of values. In APPENDIX A, we derive the equation that will allow us to solve the four possible pairs of inverse values of (2.2) by using Matlab. However, the map F is regular (=nonsingular) almost everywhere so that it follows from the inverse function theorem that its inverse is locally defined as an analytic map almost everywhere on the image of F. Consequently, we may define a sort of pseudo-action $\mathbf{Z} \times \mathbf{R}^2 \to \mathbf{R}^2$ via

$$(n, X) \mapsto F^n(X)$$

with the understanding we have to choose a particular local analytic branch of F^{-1} at each regular value of F. Perhaps one should say that the iterations of F

and the iterations of F^{-1}, when defined (almost everywhere) upon selection of an analytic local branch, comprise a smooth pseudo-dynamical system. But this is rather awkward, and if we are careful and keep in mind the above caveats — and the modification they require in such notions as orbits and unstable manifold — it shall do no harm to abuse notation in the sequel by referring to the above pseudo-action as a smooth discrete dynamical system.

2.3 Analytical Results of the LV Model

In this section, we shall formulate the analytical results of the location and types of the fixed points of F.

2.3.1 Location of Fixed Points

Let us first determine those points where F does not have a local inverse; namely, the singular or critical points. For this, we locate the zeros of the determinant of the derivative of F, F', by computing

$$\det F'(X) = \lambda\mu \begin{vmatrix} 1-2ax-by & -bx \\ -cy & 1-cx-2dy \end{vmatrix} = 0,$$

which leads to the following conic of singular points:

$$2acx^2 + 4adxy + 2bdy^2 - (2a+c)x - (2d+b)y = 1. \tag{2.5}$$

Next we find the location and types of the fixed points of F. These points $X = (x, y)$ are solutions of the equations

$$\begin{aligned} \lambda x(1-ax-by) &= x, \\ \mu y(1-cx-dy) &= y, \end{aligned}$$

which yield the following four fixed points:

$$\begin{aligned} &X_0 = (0,0), \quad X_1 = (\tfrac{\lambda-1}{a\lambda}, 0), \quad X_2 = (0, \tfrac{\mu-1}{d\mu}), \quad \text{and} \\ &X_3 = \tfrac{1}{ad-bc}\left(d(\tfrac{\lambda-1}{\lambda}) - b(\tfrac{\mu-1}{\mu}), a(\tfrac{\mu-1}{\mu}) - c(\tfrac{\lambda-1}{\lambda})\right), \end{aligned} \tag{2.6}$$

wherever the formulas make sense. For example, if $a = 0$, the second point in (2.6) does not exist unless $\lambda = 1$, in which case every point on the x-axis is fixed, if $d = 0$, the third point does not exist unless $\mu = 1$, in which case every point on the y-axis is fixed and if $ad - bc = 0$, the fourth point does not exist unless the ranks of the matrices

$$\begin{bmatrix} a & b \\ c & d \end{bmatrix} \text{ and } \begin{bmatrix} a & b & \frac{\lambda-1}{\lambda} \\ c & d & \frac{\mu-1}{\mu} \end{bmatrix}$$

are equal, in which case it corresponds to a whole line of fixed points satisfying

$$ax + by = \frac{\lambda - 1}{\lambda}.$$

2.3.2 Stability Analysis

Here we find the types of fixed points of F. The derivative at X_0 is

$$F'(X_0) = \begin{bmatrix} \lambda & 0 \\ 0 & \mu \end{bmatrix},$$

so X_0 is a sink if $\lambda, \mu < 1$, a source if $\lambda, \mu > 1$, a saddle if one of λ, μ is less than one and the other greater than one, and is degenerate if one or both of λ, μ is equal to one. If the fixed point X_1 exists, we compute that

$$F'(X_1) = \begin{bmatrix} 2 - \lambda & \frac{b}{a}(1 - \lambda) \\ 0 & \frac{\mu}{a\lambda}[\lambda(a - c) + c] \end{bmatrix},$$

with eigenvalues $2 - \lambda$ and $\frac{\mu}{a\lambda}[\lambda(a - c) + c]$. So, for example, this is a (orientation-reversing) source if $\lambda > 3$ and $\mu > a\lambda[\lambda(a - c) + c]^{-1}$. At the fixed point X_2, we find that

$$F'(X_2) = \begin{bmatrix} \frac{\lambda}{d\mu}[\mu(d - b) + b] & 0 \\ \frac{c}{d}(1 - \mu) & 2 - \mu \end{bmatrix},$$

with eigenvalues $\frac{\lambda}{d\mu}[\mu(d - b) + b]$ and $2 - \mu$. For example, if $1 < \mu < 2$ and $\lambda > d\mu[\mu(d - b) + b]^{-1}$, then X_2 is a (orientation-preserving) saddle. Finally, we compute that the eigenvalues of $F'(X_3)$ are

$$\frac{1}{2}\left[(\lambda A + \mu B) \pm \sqrt{(\lambda A - \mu B)^2 + 4\lambda\mu bc x_3 y_3}\right],$$

where x_3 and y_3 are the x- and y-coordinates of X_3, respectively, $A := 1 - 2ax_3 - by_3$ and $B := 1 - cx_3 - 2dy_3$. Note that the eigenvalues are both real whenever $x_3 y_3 \geq 0$.

It is useful to observe that both the x-axis and the y-axis are invariant manifolds for the discrete dynamical system of F. This is obvious for the forward iterations since if X has the second (first) coordinate equal to zero, then the same is true of $F(X)$. For inverse iterations, that are in general multivalued when defined, it is easy to verify that at least one determination of F^{-1} maps the x- and y-axes into themselves. Observe also that the restriction of F to either the x-axis or y-axis is either a simple linear map or is conjugate to the logistic map.

2.4 A Simple Uncoupled Case of the LV Model

Here we shall briefly consider the special uncoupled case of the LV map (2.3) with $\alpha = \beta = 0$; namely,

$$F(x, y) = (\lambda x(1 - x), \mu y(1 - y)). \tag{2.7}$$

There is really nothing new in the dynamics of (2.7) since this case is essentially determined by the logistic map owing to the fact that F is just a product of logistic maps; i.e.,

$$F = f_\lambda \times f_\mu.$$

Nevertheless, we shall point out a few of the features of the iterations of this map.

Keeping in mind the underlying theme of the LV map as a population model, it makes sense to restrict F to the first quadrant of the plane or more precisely to the square $I^2 := [0, 1] \times [0, 1]$. If both $\lambda, \mu < 1$, it is clear that $(0, 0)$, the only fixed point of the restricted map $F|_{I^2}$, is a global attractor for the discrete dynamical system. Recall the period-doubling bifurcation value sequence for the logistic map (see [28] and [41]):

$$\delta_1 = 3 < \delta_2 \simeq 3.4495 < \delta_3 \simeq 3.5441 < \ldots < \delta_n \to \delta_\infty \simeq 3.5699\,.$$

Fix $\delta_1 < \mu < \delta_2$ and let λ increase up to δ_∞. Then the iterations of $f_\lambda \times f_\mu$ experience a period-doubling cascade culminating at (μ, δ_∞) in three invariant aperiodic sets of the form

$$\begin{aligned} E_0 &= \{(x,0) : x \in S \subset [0,1]\}, \\ E_1 &= \{(x, \frac{\mu - 1}{\mu}) : x \in S \subset [0,1]\}, \\ E_2 &= \{(x,y) : x \in S, y \in \{y^{(1)}, y^{(2)}\}\}, \end{aligned}$$

where S is the usual aperiodic attractor for the logistic map f_λ obtained as the limit of its period-doubling cascade and $\{y^{(1)}, y^{(2)}\}$ is the attracting two-cycle of f_μ. The set E_2 is an aperiodic attractor of $F|_{I^2}$, while the aperiodic invariant sets, E_0 and E_1, are attractors for the restriction of F to these sets and repel nearby points off their respective horizontal lines.

Of course, one encounters chaotic dynamics for (2.7) in certain ranges of the parameters. For example, when $\lambda, \mu > 4$ the motion is chaotic on a strange repeller $R \subset I^2$ which is the Cartesian product of a pair of two-component Cantor sets. In this case the set of periodic points of $F|_R$, $Per(F|_R)$, is dense in R and contains periodic points of arbitrarily large periods. $F|_R$ has a dense orbit and it exhibits sensitive dependence on initial conditions signaled by two positive Lyapunov exponents. Chaos also occurs in less extreme forms; for example, there exist parameter values $0 < \lambda < \delta_\infty$ and $\delta_\infty < \mu < 4$ such that (2.7) has chaotic orbits having only a single nonzero Lyapunov exponent.

When $\lambda = \mu$, the map (2.7) enjoys the additional property of being symmetric with respect to the reflection $(x,y) \mapsto (y,x)$; i.e., this map is a conjugacy of F with itself. In this case F has, in addition to the x- and y-axes, the diagonal line $y = x$ as an invariant manifold and F restricted to the diagonal is also a logistic map.

The above examples illustrate the following basic fact concerning (2.7): Although it subsumes the logistic map, its behavior is actually completely determined

by the one-dimensional dynamics of the logistic map iterations. Consequently, all of its dynamical properties can be easily derived from those of the logistic map.

2.5 A Simple Coupled Case of the LV Model

In this section we shall investigate the dynamics of the simple, fully quadratic, coupled special case of the LV map given by (2.4); namely,

$$F(x,y) = (\lambda x(1-y), \mu y(1-x)). \tag{2.8}$$

As we shall see, some interesting elements of the dynamical behavior of (2.8) are also essentially logistic in nature.

We begin with some general observations. It follows from the discussion in Section 2.3.1 that the fixed points of the map defined by (2.8) are

$$\begin{aligned} &X_0 = (0,0), X_3 = (\tfrac{\mu-1}{\mu}, \tfrac{\lambda-1}{\lambda}), \\ &\text{all points of the } x\text{-axis if } \lambda = 1, \text{ and} \\ &\text{all points of the } y\text{-axis if } \mu = 1. \end{aligned} \tag{2.9}$$

The orbit structure for points in the unit square I^2 is particularly simple when $\lambda, \mu < 1$.

Lemma 1 *If $0 < \lambda, \mu < 1$, the unit square I^2 is invariant with respect to the map F defined by (2.8). Moreover, $(0,0)$ is a global (exponential) attractor for $F|_{I^2}$.*

Proof: We first verify that $F(I^2) \subset I^2$. But this is easily accomplished because $0 \leq x, y \leq 1$ implies that $0 \leq \lambda x(1-y) \leq \lambda < 1$ and $0 \leq \mu y(1-x) \leq \mu < 1$ owing to the hypothesis.

As for the remainder of the theorem, we first note that $(0,0)$ is the only fixed point of F in I^2. A simple computation shows that $F'(0)$ has eigenvalues λ and μ, so $(0,0)$ is a sink. It is obvious from the invariance of the x- and y-axes that positive semiorbits starting on the coordinate axes in I^2 converge exponentially to $(0,0)$ with

exponents λ and μ, respectively. The exponential convergence to $(0,0)$ of iterations of F beginning in the interior of I^2 can be immediately inferred from the following inequality

$$\lambda^2 x^2(1-y)^2 + \mu^2 y^2(1-x)^2 < \lambda^2 x^2 + \mu^2 y^2 \leq \max\{\lambda^2, \mu^2\}(x^2+y^2).$$

Thus the proof is complete. □

If $\lambda = \mu$, we have a special symmetric case of (2.8) where logistic dynamics is the dominant feature. In this case, F is symmetric with respect to the reflection $(x,y) \to (y,x)$ in the sense that it is conjugate to itself via this linear isomorphism. As a consequence, the diagonal $y = x$ is an additional invariant manifold for F, and the restriction of F to the diagonal is the logistic map $f : \mathbf{R} \to \mathbf{R}$ defined by

$$f(x) := \lambda x(1-x).$$

Thus as λ is varied, F experiences the complete range of one-dimensional dynamics exhibited by the logistic map, including chaos for $\lambda > \delta_\infty$. In fact, in the symmetric case, it is possible to characterize the global dynamics of (2.8) and in doing so establish that the only really interesting behavior derives from that of the logistic map. A key ingredient is the following simple result.

Lemma 2 *Define the lines*

$$L_\sigma := \{(x,y) \in \boldsymbol{R}^2 : y = x + \sigma, \sigma \in \boldsymbol{R}\}.$$

Then if $\lambda = \mu$ in (2.8), $F(L_\sigma) \subset L_{\lambda\sigma}$.

Proof: This inclusion follows immediately from the fact that

$$\lambda(x+\sigma)(1-x) = \lambda x(1-x-\sigma) + \lambda\sigma,$$

and this completes the proof. □

The next result illustrates how one may obtain a global description of the dynamics in the symmetric case. A simple proof can easily be fashioned using the above remarks and Lemma 2.

Lemma 3 *If $\lambda = \mu > 1$ in (2.8), the dynamical system of iterations of F have the following properties:*

(i) *F has precisely two fixed points: a source at $(0,0)$ and a fixed point at $(\frac{\lambda-1}{\lambda})(1,1)$ that bifurcates from a saddle into a source at $\lambda = 3$.*

(ii) *F has precisely three linear, codimension-one, invariant manifolds: the x-axis, the y-axis and the diagonal $y = x$. F restricted to both the x- and y-axes is an expanding linear map of the form $x \to \lambda x$, while the restriction of F to the diagonal is the logistic map $f(x) = \lambda x(1-x)$.*

(iii) *The invariant diagonal is a global repelling set; in fact, $d(F^n(X), L_\sigma) = \lambda^n d(X, L_\sigma)$ for all $X \subset \boldsymbol{R}^2$ and $n \subset \boldsymbol{Z}_+$, where d denotes the distance between the point and the set.*

(iv) *The dynamics of F exhibit logistic period-doubling bifurcation and chaos along the diagonal as λ is increased.*

Proof: Property (i) is a direct result from the analysis shown in Section 2.3.1. The three manifolds in Property (ii) are in fact linear and invariant by virtue of their respective locations. Property (iii) is easily understood since for $\lambda > 1$ and as $n \to \infty$, $d(F^n(X), L_\sigma) = \lambda^n d(X, L_\sigma) \to \infty$. Along the diagonal, $y = x$, we obtain the logistic map $f : \mathbf{R} \to \mathbf{R}$ defined by

$$f(x) := \lambda x(1-x),$$

and it exhibits logistic periodic-doubling bifurcation and chaos as λ increases. This completes the proof. □

By way of contrast, let us consider the highly asymmetrical case where $\lambda = 4$ and $\mu = 3/2$. This case does not exhibit any chaotic behavior in the square I^2. To see this, we first note that the only fixed points are the origin and

$$X_3 = (\frac{1}{3}, \frac{3}{4}),$$

both of which lie in I^2. It is easy to see that $X_0 = (0,0)$ is a source and that X_3 is a saddle point with eigenvalues $1 \pm \sqrt{\frac{3}{2}}$. The stable and unstable manifolds of $F'(X_3)$, respectively, are the lines

$$\begin{aligned} W_l^s &= \{(x,y) : -\sqrt{\tfrac{3}{2}}(x - \tfrac{1}{3}) + \tfrac{4}{3}(y - \tfrac{3}{4}) = 0\}, \text{ and} \\ W_l^u &= \{(x,y) : \sqrt{\tfrac{3}{2}}(x - \tfrac{1}{3}) + \tfrac{4}{3}(y - \tfrac{3}{4}) = 0\}, \end{aligned} \tag{2.10}$$

which are local approximations of the stable manifold W^s and the unstable manifold W^u of F at X_3, respectively. It is also useful to note that F is singular along the line

$$x + y = 1,$$

and that $F(x,y) = (u,v)$ has at most a pair of solutions given by

$$x = \tfrac{1}{18}\left[(3 + \tfrac{3}{4}u - 2v) \pm \sqrt{(3 + \tfrac{3}{4}u - 2v)^2 - 3u}\right],$$

$$y = \tfrac{2v}{3(1-x)},$$

wherever these formulas make sense and have real solutions.

Horizontal and vertical lines through X_3 subdivide I^2 into the following rectangles:

$$\begin{aligned} I_1 &:= \{(x,y) : 1/3 \le x \le 1, 0 \le y \le 3/4\}, \\ I_2 &:= \{(x,y) : 1/3 \le x \le 1, 3/4 \le y \le 1\}, \\ I_3 &:= \{(x,y) : 0 \le x \le 1/3, 3/4 \le y \le 1\}, \\ I_4 &:= \{(x,y) : 0 \le x \le 1/3, 0 \le y \le 3/4\}. \end{aligned}$$

Observe that there is a closed disk $\triangle$ centered at X_3 and contained in the interior of I^2 of sufficiently small radius such that

$$\begin{aligned} W^s \cap (\triangle \backslash X_3) \subset \text{int } (I_2 \cup I_4), \text{ and} \\ W^u \cap (\triangle \backslash X_3) \subset \text{int } (I_1 \cup I_3). \end{aligned}$$

Moreover, it is easy to see that the following properties obtain:

$$\begin{aligned}
(x_n, y_n) \in \text{int } I_1 &\Rightarrow x_{n+1} = a_n x_n,\ y_{n+1} = b_n y_n, \\
&\quad \text{with } a_n > 1 \text{ and } 0 < b_n < 1; \\
(x_n, y_n) \in \text{int } I_2 &\Rightarrow x_{n+1} = a_n x_n,\ y_{n+1} = b_n y_n, \\
&\quad \text{with } 0 < a_n, b_n < 1; \\
(x_n, y_n) \in \text{int } I_3 &\Rightarrow x_{n+1} = a_n x_n,\ y_{n+1} = b_n y_n, \\
&\quad \text{with } 0 < a_n < 1 \text{ and } b_n > 1; \\
(x_n, y_n) \in \text{int } I_4 &\Rightarrow x_{n+1} = a_n x_n,\ y_{n+1} = b_n y_n, \\
&\quad \text{with } a_n, b_n > 1.
\end{aligned}$$

Using the above properties, it is easy to see the following facts regarding the dynamics of F: The stable manifold W^s is a smooth open manifold and its closure $\overline{W}^s$ is contained in I^2 and satisfies $\overline{W}^s \backslash W^s = \{(0,0),(1,1)\}$. The unstable manifold W^u is a smooth open manifold that exits I^2 at points along the rightmost edge of I_1 and the uppermost edge of I_3 and then never returns to I^2. For points not on W^s or W^u; i.e., for $X \subset I^2 \backslash (\overline{W}^s \cup W^u)$, the positive semiorbits all eventually exit I^2 through its upper or right edge. As a matter of fact, the same type of analysis can be applied to prove the following more general result.

Lemma 4 *Let the LV map (2.8) be such that $\lambda, \mu > 1$ and $(\lambda - 1)(\mu - 1) < 4$. Then the map F has the following dynamical properties on I^2:*

(i) *F has precisely two fixed points: a source at $X_0 = (0,0)$ and a saddle point $X_3 = \left(\frac{\mu-1}{\mu}, \frac{\lambda-1}{\lambda}\right)$ in I^2 and F has no other periodic points in I^2.*

(ii) *The stable manifold W^s for the point X_3 is a smooth, open 1-dimensional submanifold of $\boldsymbol{R}^2$ contained in int I^2 and its closure contains the additional points $X = (0,0)$ and $X = (1,1)$.*

(iii) *The unstable manifold W^u for the point X_3 is a smooth, open one-dimensional submanifold of $\boldsymbol{R}^2$ that is unbounded and exits I^2 at points on the upper and right edges and then never returns to I^2.*

(iv) *The iterations of any point in $I^2 \backslash (\overline{W}^s \cup W^u)$ under F eventually exit I^2 through its upper or right edge.*

The rather tame dynamical behavior described in Lemma 4 is illustrated in Fig. 2.1 for the case $\lambda = 4, \mu = 1.5$.

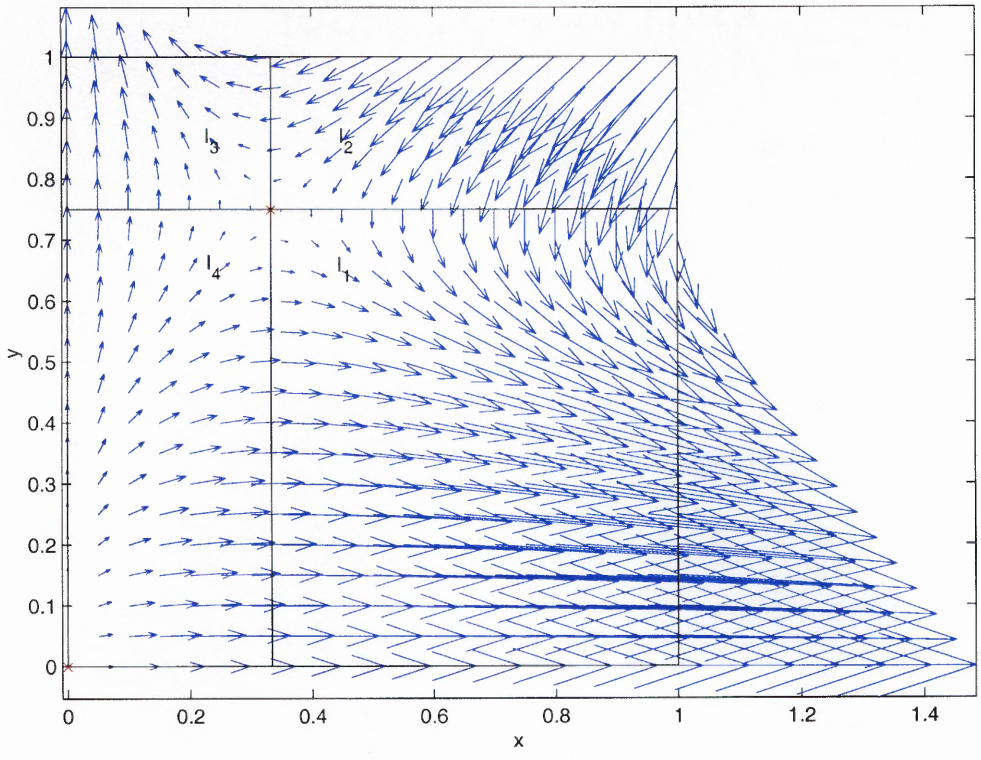

Figure 2.1 Dynamics of (2.8) for $\lambda = 4, \mu = 1.5$. The fixed points are $(0,0)$ and $(0.\bar{3}, 0.75)$ in two red 'x'-marks with eigenvalues $(4, 1.5)$ and $(2.2247, -0.2247)$, respectively.

We conclude this section with a conjecture about the dynamics of F in the case where the inequality on $(\lambda - 1)(\mu - 1)$ in Lemma 4 is reversed. It appears that the only complicated behavior in this case is of the one-dimensional logistic variety. In particular, it should be possible to prove the following result using graph transform techniques ([16]).

Conjecture 5 *If the LV map (2.8) is such that* $\lambda, \mu > 1$ *and* $(\lambda - 1)(\mu - 1) > 4$, *then it has the following dynamical properties on* I^2*:*

(i) *The only fixed points of* F *are a source at the origin and a source at* $\left(\frac{\mu-1}{\mu}, \frac{\lambda-1}{\lambda}\right)$.

(ii) *There exists a one-dimensional, F-invariant C^1-manifold of the form $M = \{(x, \varphi(x)) : \varphi : \boldsymbol{R} \to \boldsymbol{R}\}$ passing through the fixed points of F such that φ is monotone increasing and the restriction $F|_M$ is a unimodular map exhibiting the same range of motion as the logistic map. In particular, $F|_M$ has chaotic dynamics when $\lambda + \mu$ is sufficiently large.*

(iii) *The iterations of any point $X \subset I^2 \backslash M$ eventually leave I^2 and never return.*

Part (i) of this conjecture is trivial as shown in Section 2.3.1. The tricky part to prove is (ii), but if this can be done, it should be relatively easy to verify (iii). Figure 2.2 supports this conjecture for the case $\lambda = 4, \mu = 3.5$.

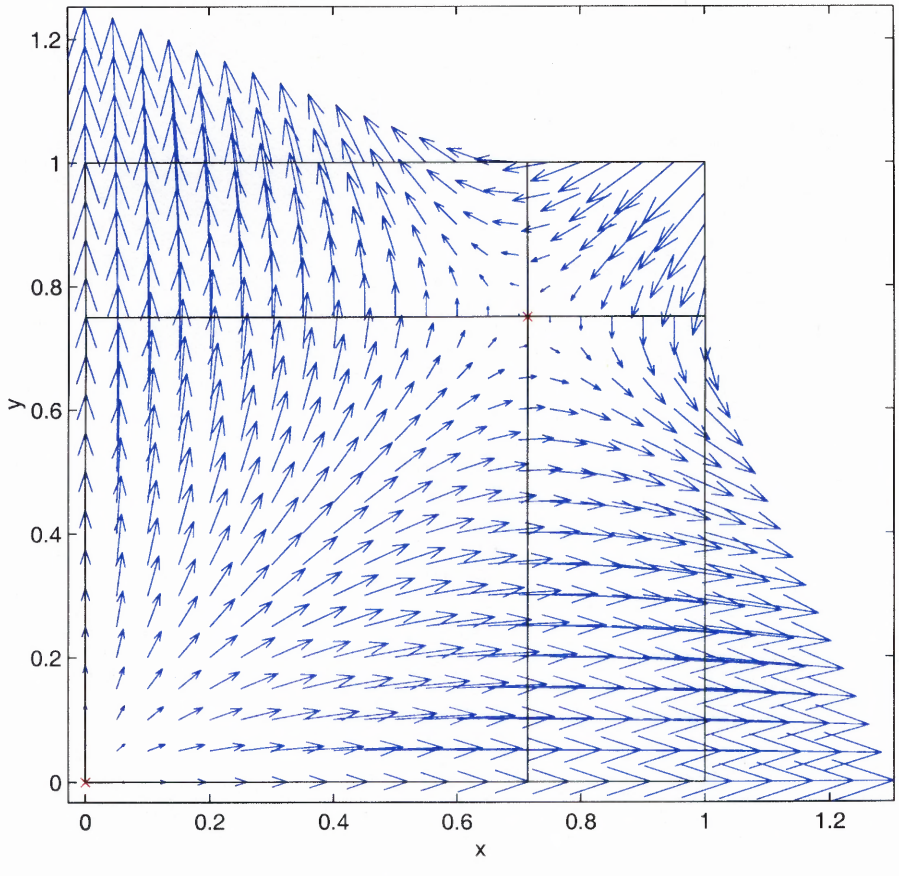

Figure 2.2 Dynamics of (2.8) for $\lambda = 4, \mu = 3.5$. The fixed points are $(0, 0)$ and $(0.7143, 0.75)$ in two red 'x'-marks with eigenvalues $(4, 3.5)$ and $(3.7386, -1.7386)$, respectively.

2.6 Additional Chaotic Regimes of the LV Model

Here we examine some interesting dynamical regimes for (2.3), which represents a fairly general form of the LV map that we repeat for convenience as

$$F(x,y) := (\lambda x(1-x-\alpha y), \mu y(1-\beta x-y)), \tag{2.11}$$

where the parameters α, β, λ and μ are all positive numbers. First we summarize some basic features of this map and its dynamics. The number and types of the fixed points of F depends on the parameters. We illustrate this with a few cases and leave the remaining cases for future studies.

(C1) $\lambda \neq 1, \mu \neq 1$ and $\alpha\beta \neq 1$: In this case, F has four fixed points; namely, $X_0 = (0,0), X_1 = (\frac{\lambda-1}{\lambda}, 0), X_2 = (0, \frac{\mu-1}{\mu})$ and $X_3 = \frac{1}{1-\alpha\beta}\left(\frac{\lambda-1}{\lambda} - \alpha(\frac{\mu-1}{\mu}), \frac{\mu-1}{\mu} - \beta(\frac{\lambda-1}{\lambda})\right)$. The fixed point X_0 is a sink if $\lambda, \mu < 1$, a source if $\lambda, \mu > 1$ and a saddle if $\lambda < 1 < \mu$ or $\mu < 1 < \lambda$.

(C2) $\lambda = 1, \mu \neq 1$ and $\alpha\beta \neq 1$: The fixed points of F are $X_0 = X_1$, X_2 and $X_3 = \frac{1}{1-\alpha\beta}(\frac{\mu-1}{\mu})(-\alpha, 1)$, and X_2 is a saddle if one of $\frac{\lambda}{\mu}|\alpha - (\alpha-1)\mu|$ and $|2-\mu|$ is less than one and the other is greater than one.

(C3) $\lambda \neq 1, \mu \neq 1, \alpha\beta = 1$ and $(\frac{\mu-1}{\mu}) - \beta(\frac{\lambda-1}{\lambda}) \neq 0$: Then X_0, X_1 and X_2 are the only fixed points of F and X_1 is a source if both $|2-\lambda|$ and $\frac{\mu}{\lambda}|\beta - (\beta-1)\lambda|$ are greater than one.

(C4) $\lambda \neq 1, \mu \neq 1, \alpha\beta = 1$ and $(\frac{\mu-1}{\mu}) - \beta(\frac{\lambda-1}{\lambda}) = 0$: In this case, X_0 is a fixed point of F and every point on the line $x + \alpha y = \frac{\lambda-1}{\lambda}$ is fixed. Moreover, all points on this line are degenerate fixed points.

As usual, both the x-axis and y-axis are F-invariant and, as we shall demonstrate in the sequel, F may have an additional distinguished invariant set.

When $\lambda, \mu < 1$, the positive semiorbits of F starting in I^2 all converge to 0 for certain ranges of the parameters α and β. But it is useful to note that, unlike the

case described in Lemma 1, some of the iterations may belong to the complement of I^2. The restriction of F to the x- and y-axes are both logistic maps, so typical logistic map bifurcation and chaos occur along the coordinate axes. It is easy to see that when $\lambda = \mu$ and $\alpha = \beta$, the diagonal $y = x$ is an additional F-invariant set. The restriction of F to the diagonal in this case is the logistic map $x \mapsto \lambda x[1 - (\alpha + 1)x]$, so it follows that F can have a one-dimensional chaotic regime distinct from those that may occur along the coordinate axes. Thus we see that the map (2.11) can exhibit one-dimensional chaotic behavior of the logistic type just like those of the more specialized LV maps that we considered in the preceding sections. It is natural to ask if (2.11) is capable of dynamical behavior that is chaotic in a form different from that of the logistic map and that is intrinsically two-dimensional? We shall devote the remainder of this section proving that this question has an affirmative answer.

In order to prove the existence of fully two-dimensional chaotic regimes, it is convenient to first introduce some notation and discuss some properties of (2.11). We shall assume in the remainder of this section that the parameters in (2.11) are restricted to the following ranges:

$$0.2 < \alpha < 0.3,\ 0.7 < \beta < 0.9,\ 2 < \lambda < 2.2,\ 3.5 < \mu < 4. \tag{2.12}$$

Then according to **(C1)**, F has four fixed points:

$$X_0 = (0,0),\ \ X_1 = (\tfrac{\lambda-1}{\lambda}, 0),\ \ X_2 = (0, \tfrac{\mu-1}{\mu}),\ \text{ and}$$

$$X_3 = \tfrac{1}{1-\alpha\beta}\left(\tfrac{\lambda-1}{\lambda} - \alpha(\tfrac{\mu-1}{\mu}), \tfrac{\mu-1}{\mu} - \beta(\tfrac{\lambda-1}{\lambda})\right).$$

In this case, where the parameter ranges are defined in (2.12), X_0 is a source, X_1 is an orientation-reversing saddle with its unstable manifold along the x-axis, X_2 is an orientation-reversing source and X_3 is an orientation-reversing saddle. We note here that it is easy to verify that the x-component of X_1 is greater than that of X_3.

Observe that the restriction of F to the x-axis is the logistic map

$$f_1(x) := F(x,0) = \lambda x(1-x),$$

with fixed points at $x = 0$ and $x = \frac{\lambda-1}{\lambda}$ and the restriction of F to the y-axis is the logistic map

$$f_2(y) := F(0,y) = \mu y(1-y),$$

with fixed points at $y = 0$ and $y = \frac{\mu-1}{\mu}$. We note that the line

$$L_1 := \{(x,y) : 1 - \beta x - y = 0\}, \tag{2.13}$$

which passes through the points (0,1) and (1,1-β), is mapped onto the x-axis by F.

Our intention is to define a trapezoidal region in I^2 that is bounded below by the x-axis and above by the line L_1 defined in (2.13), has its remaining two sides vertical, contains the fixed point X_3 in its interior, and on which F acts like a (orientation-reversing) horseshoe map. We denote this trapezoidal region by R_0 and define it as follows:

$$R_0 := \{(x,y) : \tfrac{\lambda-1}{\lambda} - a \le x \le \tfrac{\lambda-1}{\lambda} + b,\ 0 \le y \le 1 - \beta x\},$$

$$\text{where} \tag{2.14}$$

$$0.08 \le a \le 0.12,\ b = \tfrac{2a}{3}.$$

Owing to (2.12), it is easy to verify that X_3 is in the interior of R_0. Of course, X_1 lies on the bottom edge of R_0 strictly between its endpoints (vertices) which we denote by

$$(\xi_1, \eta_1) := \left(\tfrac{\lambda-1}{\lambda} - a, 0\right) \text{ and}$$

$$(\xi_2, \eta_2) := \left(\tfrac{\lambda-1}{\lambda} + b, 0\right).$$

The remaining vertices of R_0, in counterclockwise order, are

$$(\xi_3, \eta_3) := \left(\tfrac{\lambda-1}{\lambda} + b, 1 - \beta(\tfrac{\lambda-1}{\lambda} + b)\right) \text{ and}$$

$$(\xi_4, \eta_4) := \left(\tfrac{\lambda-1}{\lambda} - a, 1 - \beta(\tfrac{\lambda-1}{\lambda} - a)\right).$$

We compute that

$$F(\xi_1, \eta_1) = \left((1 - \tfrac{1}{\lambda}) + (\lambda - 2)a + \lambda a^2, 0\right),$$

$$F(\xi_2, \eta_2) = \left((1 - \tfrac{1}{\lambda}) - (\lambda - 2)b - \lambda b^2, 0\right),$$

$$F(\xi_3, \eta_3) = \left((1 - \tfrac{1}{\lambda}) - (\lambda - 2)b - \lambda b^2 - \alpha\lambda(1 + b - \tfrac{1}{\lambda})(1 - (1 + b - \tfrac{1}{\lambda})\beta), 0\right) \text{ and}$$

$$F(\xi_4, \eta_4) = \left((1 - \tfrac{1}{\lambda}) + (\lambda - 2)a + \lambda a^2 - \alpha\lambda(1 - a - \tfrac{1}{\lambda})(1 - (1 - a - \tfrac{1}{\lambda})\beta), 0\right).$$

Hence the F-images of the bottom edge and top edge of R_0 are two disjoint closed intervals in the interior of the bottom edge of R_0, with the image of the top edge of R_0 lying to the left of the image of the bottom edge of R_0 (see Figure 2.3).

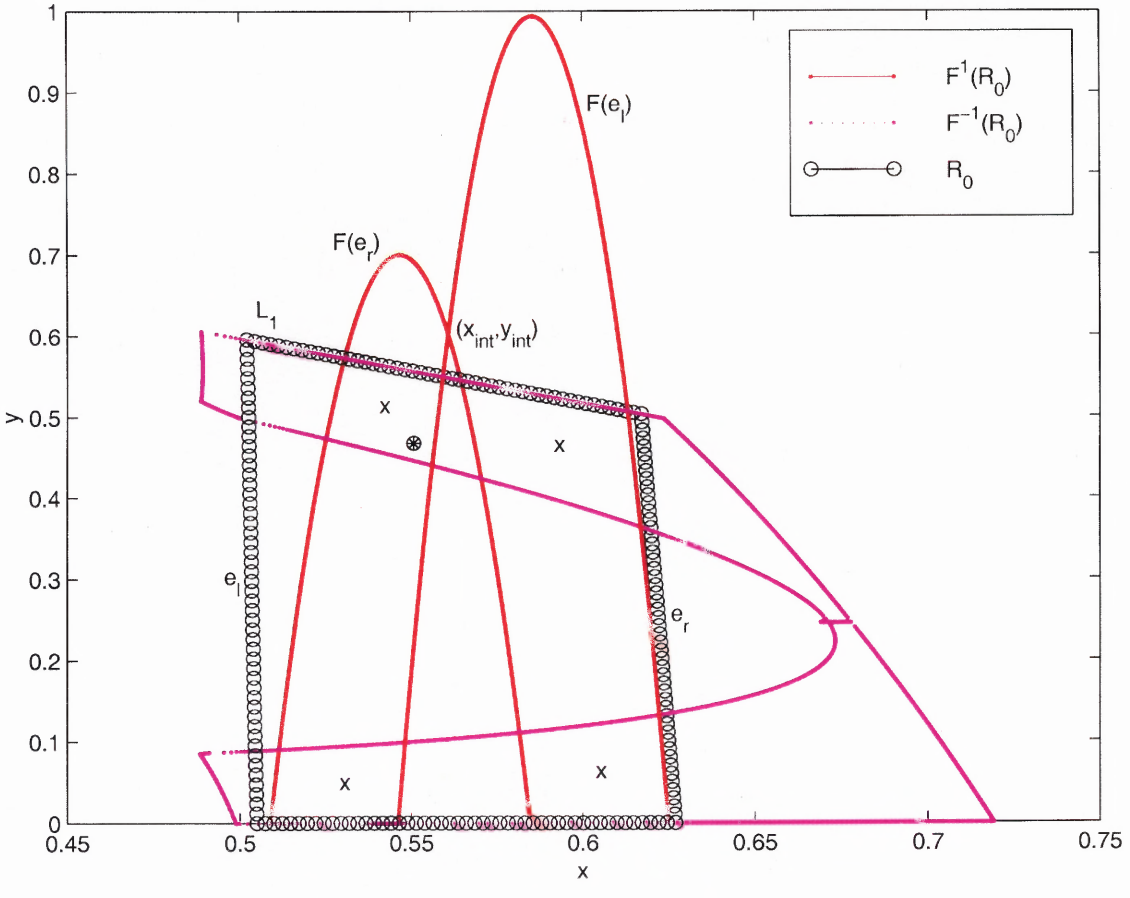

Figure 2.3 The action of F^1 and F^{-1} on R_0. Λ_1 is marked by 'x'.

The image of the left edge of R_0 is the parabolic curve defined as

$$\begin{aligned} F(e_l) &:= \left((\tfrac{\lambda-1}{\lambda} - a, y) : 0 \le y \le 1 - \beta(\tfrac{\lambda-1}{\lambda} - a)\right) \\ &:= \{\left(\lambda(1 - a - \tfrac{1}{\lambda})(a + \tfrac{1}{\lambda} - \alpha y), \mu y(1 - y - \beta(1 - a - \tfrac{1}{\lambda}))\right) : \\ &\quad 0 \le y \le 1 - \beta(\tfrac{\lambda-1}{\lambda} - a)\} \end{aligned}$$

and image of the right edge of R_0 is the parabolic curve defined as

$$\begin{aligned} F(e_r) &:= \left((\tfrac{\lambda-1}{\lambda} + b, y) : 0 \le y \le 1 - \beta(\tfrac{\lambda-1}{\lambda} + b)\right) \\ &:= \{\left(\lambda(1 + b - \tfrac{1}{\lambda})(\tfrac{1}{\lambda} - b - \alpha y), \mu y(1 - y - \beta(1 + b - \tfrac{1}{\lambda}))\right) : \\ &\quad 0 \le y \le 1 - \beta(\tfrac{\lambda-1}{\lambda} + b)\} \end{aligned}$$

An example of these parabolas is shown in Figure 2.3. It can be shown that for the case under consideration (as defined in (2.12)) both of the parabolas $F(e_l)$ and $F(e_r)$ attain their maximum heights at points in I^2 above the line L_1. Moreover, the maximum height of $F(e_l)$ is greater than the maximum height of $F(e_r)$ and these two parabolic segments have precisely one intersection point — a point that lies above the line L_1. In APPENDIX B, we derive the location of the intersection point of the parabolas $F(e_l)$ and $F(e_r)$ by solving two equations with two unknowns and yield the solution

$$x_{int} := \lambda x_l x_r \quad \textit{and} \quad y_{int} := \tfrac{1}{\alpha}(1 - x_l - x_r)$$

where

$$x_l := \tfrac{\lambda-1}{\lambda} - b \quad \textit{and} \quad x_r := \tfrac{\lambda-1}{\lambda} + a.$$

Consequently, we conclude that $F(R_0)$ is obtained from R_0 by squeezing (essentially in the horizontal direction), stretching (approximately in the vertical direction), applying a single twist and then folding over so that it intersects R_0 in two essentially vertical curvilinear rectangular regions as illustrated in Figure 2.3 and 2.4. Hence, it is quite natural to refer to the restriction of F to R_0 as a *twisted horseshoe.*

In preparation for the proof of our main theorem that relies on making what is by now a rather obvious connection with the standard horseshoe map of Smale (see [5], [8] and [17]) and its symbolic dynamics, we need to introduce some additional notation. Define

$$\begin{aligned} \Lambda_0 &:= R_0 \\ \Lambda_n &:= F^n(\Lambda_0) \cap \Lambda_0 \end{aligned} \tag{2.15}$$

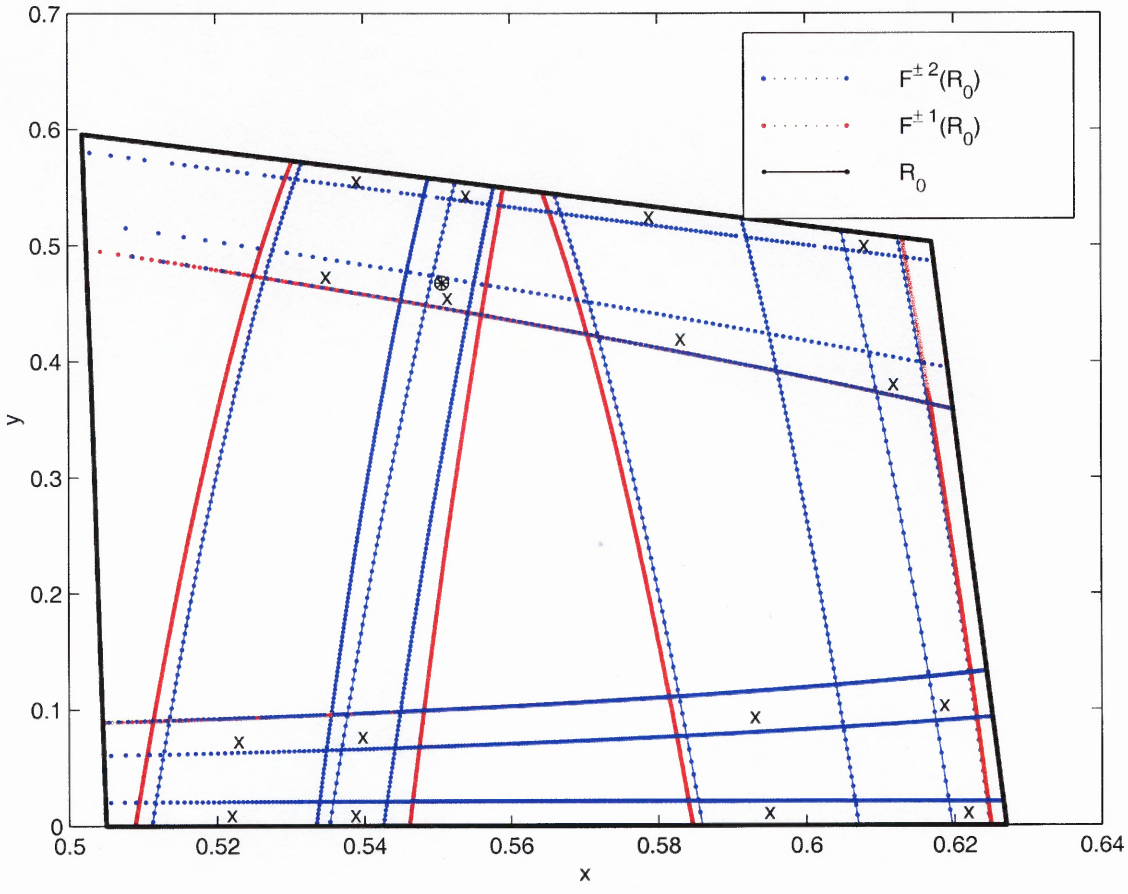

Figure 2.4 The action of $F^{\pm 2}$ and $F^{\pm 1}$ on R_0. Λ_2 is marked by 'x'.

for all positive integers n. Observe that Λ_n has 2^n essentially vertical curvilinear rectangular components in Λ_0 for all $n \geq 0$, and the width of these components goes to zero as $n \to \infty$ at an approximate rate of $(\lambda - 2)^n$. Now define Λ_{10} to be the leftmost component of Λ_1 in Λ_0 and Λ_{11} to be the rightmost component of Λ_1 in Λ_0. Continuing in this fashion, we inductively define $\Lambda_{1(s0)}$ where (s) is a binary sequence of length $k-1$, to be the leftmost component of Λ_k in $\Lambda_{1(s)}$ and $\Lambda_{1(s1)}$ to be the rightmost component of Λ_k in $\Lambda_{1(s)}$. In this manner we uniquely define the region $\Lambda_{1(s)}$ for all finite binary strings (s).

We need to exercise some care in extending the definition (2.15) to negative integers, if we are to realize our goal of completing the analog between our twisted

horseshoe and the standard horseshoe. Toward this end, we inductively define the sets

$$\begin{aligned} \Lambda_{-1} &:= F^{-1}(\Lambda_0) \cap \Lambda_0 \\ \Lambda_{-n} &:= F^{-n}(\Lambda_0) \cap \Lambda_0, \end{aligned} \tag{2.16}$$

for all positive integers $n \geq 2$. Here $F^{-1}(\Lambda_0)$ is the preimage of Λ_0 under F and not, strictly speaking, the image of Λ_0 under F^{-1}. The reason for this is that the relation F^{-1} is not well-defined as a function. $F^{-n}(\Lambda_0)$ is then unambiguously defined via induction as the preimage of $F^{-(n-1)}(\Lambda_0)$ under F. It is easy to verify that Λ_{-1} has two disjoint components in Λ_0, each of which is a nearly horizontal, curvilinear rectangle, where the uppermost component shares its upper edge (in the line L_1) with Λ_0 and the lowermost component shares its lower edge (along the x-axis) with Λ_0. In fact, it is straightforward to show that Λ_{-n} has 2^n essentially horizontal curvilinear components in Λ_0 for each $n \geq 1$ such that the uppermost component shares its upper edge with Λ_0, the lowermost component shares its lower edge with Λ_0 and the thickness (or height) of these components goes to zero as $n \to \infty$ at an approximate rate of μ^{-n} (see Figure 2.3 and 2.4). Define Λ_{-10} to be the uppermost component of Λ_{-1} in Λ_0 and Λ_{-11} to be the lowermost component of Λ_{-1} in Λ_0. Proceeding in this fashion, we inductively define $\Lambda_{-1(s)}$ for all binary strings (s) as follows: Let (s) be a binary string of length $k-1$. Define $\Lambda_{-1(s0)}$ to be the uppermost component of Λ_{-k} in $\Lambda_{-1(s)}$ and $\Lambda_{-1(s1)}$ to be the lowermost component of Λ_{-k} in $\Lambda_{-1(s)}$.

Now we have assembled just about all of the information needed to prove our main theorem. The set defined by

$$\begin{aligned} \Lambda &:= \bigcap\{F^n(\Lambda_0) \cap \Lambda_0 : n \in \mathbf{Z}\} \\ &= \bigcap\{\Lambda_n : n \in \mathbf{Z}\} \\ &= \bigcap\{\Lambda_{1(s)} \cap \Lambda_{-1(s)} : (s) \text{ a binary string}\} \end{aligned} \tag{2.17}$$

is obviously a compact, F-invariant set contained in Λ_0, and it is straightforward to show that this set is homeomorphic with

$$K \times K,$$

where K is the standard 2-component Cantor set. Observe that the fixed points X_1 and X_3 both belong to Λ and that for any point X in the bottom edge or top edge of Λ_0, respectively, $F^n(X) \in$ bottom edge of Λ_0 for all $n \geq 0$ or $n \geq 1$, and $F^n(X) \to X_1$ as $n \to \infty$.

Theorem 6 *Let the parameters in the map (2.11) satisfy (2.12) and let Λ be as defined in (2.17). Then the following properties obtain:*

(i) *Λ is a compact, F-invariant subset contained in $\boldsymbol{R}^2$.*

(ii) *The restriction of F to Λ, F_Λ, is topologically conjugate to the shift map*

$$\sigma : 2^{\boldsymbol{Z}} \to 2^{\boldsymbol{Z}}.$$

(iii) *The forward iterations under F of points in*

$$\mathcal{R} := \Lambda_0 \backslash \cap \{\Lambda_{-1(s)} : (s) \text{ a binary string}\}$$

eventually leave Λ_0 and never return, while the forward iterations under F of points in

$$\mathcal{A} := \cap\{\Lambda_{-1(s)} : (s) \text{ a binary string}\} = \Lambda_0 \backslash \mathcal{R}$$

converge to Λ as $n \to \infty$.

Proof: Property (i) is obviously a direct consequence of the definition (2.17). In order to prove (ii), one simply uses the itineraries of the points in Λ in what by now is a quite standard and routine argument. For example, the method of proof is very nicely outlined by Devaney[5] for the Hénon map in a series of exercises. We shall

describe a few of the details. It helps to observe that owing to the definition of Λ, although F is not invertible on Λ_0, the restriction F_Λ has a smooth inverse F_Λ^{-1}. The desired conjugacy $\varphi : \Lambda \to 2^{\mathbf{Z}}$, the itinerary map, is defined as follows:

$$\varphi(x)(m) := \begin{cases} 0, & \text{if } F_\Lambda^m(x) \in \Lambda_{10} \\ 1, & \text{if } F_\Lambda^m(x) \in \Lambda_{11}, \end{cases} \tag{2.18}$$

where Λ_{10} and Λ_{11} are as defined above after the formula (2.15). It is then a straightforward exercise to verify that φ is a homeomorphism. Whence the fact that φ is a topological conjugacy between F_Λ and the shift map is a trivial consequence of its very definition. It is worth noting that under this conjugacy the fixed point X_3 corresponds to the element of $2^{\mathbf{Z}}$ having a constant value of zero and X_1 corresponds to the function having a constant value of one.

To prove (iii), we first note that it is an immediate consequence of the construction of the sets $\Lambda_{-1(s)}$ that any point in

$$\mathcal{R} = \Lambda_0 \setminus \cap \{\Lambda_{-1(s)} : (s) \textit{ a binary string}\}$$

must leave Λ_0 and never return after finitely many forward iterations. Therefore it remains to show that if

$$X \in \mathcal{A} = \cap\{\Lambda_{-1(s)} : (s) \textit{ a binary string}\},$$

then $F^n(X) \to \Lambda$ as $n \to \infty$. Of course, it is an immediate consequence of the definition of the sets $\Lambda_{-1(s)}$ that $F^n(X) \in \Lambda_0$ for all nonnegative integers n. The result is obviously true if $X \in \Lambda$, so we may assume that

$$X \in \mathcal{A} \setminus \left(\Lambda_0 \setminus \cap \{\Lambda_{1(s)} : (s) \textit{ a binary string}\}\right).$$

Clearly, $F^n(X) \in \mathcal{A}$ for all $n \geq 0$. Suppose that the distance from X to Λ is $d > 0$. Then as $F^n(X) \in \Lambda_0$ for all $n \geq 0$, and since it follows from our construction that F contracts Λ_0 horizontally by a scale factor not exceeding $(\lambda - 2)$, we readily infer that

the distance from $F^n(X)$ to Λ can be no greater than $(\lambda - 2)^n d$. Hence $F^n(X) \to \Lambda$ as $n \to \infty$, and the proof is complete. □

We note that by interchanging λ and μ and α and β in (2.12), it is possible to create twisted horseshoe behavior for F in a trapezoidal region bounded by a line segment on the positive y-axis instead of the positive x-axis. The parameter ranges for twisted horseshoe dynamics are by no means maximal; such behavior can also be observed for parameter values lying outside of the intervals specified in (2.12). For example, the parameter values used in drawing Figures 2.3 and 2.4 are as follows: $\alpha = 0.1055, \beta = 0.8055, \lambda = 2.5$ and $\mu = 11.25$.

Theorem 6 shows that the basin of attraction of Λ has (Lebesgue) measure zero and that almost all nearby points are repelled by Λ. This propensity for points near Λ to exit Λ_0 after finitely many forward iterations by F is illustrated in Tables 2.1 - 2.3. In practical terms, twisted horseshoe dynamics is not likely to be observed for competing species whose behavior can actually be modeled by a Lotka-Volterra map — it would require a fortuitous initial positioning of the two species to produce this type of chaos. More probably, if the species start near Λ, they will at least for a reasonable period of time evince the dynamics that appears to be of the chaotic, twisted horseshoe type. Such short-time correlation with this type of chaotic regime may provide at least a partial verification of the discrete Lotka-Volterra model.

Here we list three tables showing iterations of points in six different locations. If the initial point is located near the x-axis or the saddle, X_3, more iterations are generated than for points are relatively far from both X_3 and the x-axis.

i	x(i)	y(i)	i	x(i)	y(i)
	0.500000000	0.000001000		0.550675210	0.467542035
1	0.624999868	0.000006719	1	0.550673978	0.467543058
2	0.585936475	0.000037534	2	0.550674294	0.467543918
3	0.606531505	0.000222950	3	0.550674050	0.467538921
4	0.596591930	0.001282225	4	0.550674868	0.467561238
5	0.601473238	0.007474517	5	0.550671318	0.467462702
6	0.598072208	0.042720128	6	0.550686967	0.467897419
7	0.594215866	0.228541703	7	0.550617932	0.465977907
8	0.566990357	0.752861151	8	0.550922697	0.474420345
9	0.501195083	-1.775008454	9	0.549581140	0.436646287
			10	0.555561512	0.592744572
			11	0.530427820	-0.268397953

Table 2.1 Left: Iterations of point near x-axis. Right: Iterations of point near the saddle, X_3.

i	x(i)	y(i)	i	x(i)	y(i)
	0.610000000	0.500000000		0.570000000	0.300000000
1	0.514306250	0.048628125	1	0.567648750	0.812919375
2	0.617892007	0.293828377	2	0.491850976	-2.470709909
3	0.542368765	0.689077680			
4	0.521939821	-0.976424348			

Table 2.2 Left: Iterations of point in $R_0 \cap F^1(R_0)$. Right: Iterations of point not in $R_0 \cap F^1(R_0)$.

i	x(i)	y(i)	i	x(i)	y(i)
	0.590000000	0.300000000		0.560000000	0.300000000
1	0.558066250	0.758548125	1	0.571690000	0.840105000
2	0.504920098	-1.775604145	2	0.485477608	-2.841037323

Table 2.3 Left: Iterations of point in $R_0 \cap F^1(R_0) \cap F^2(R_0)$. Right: Iterations of point not in $R_0 \cap F^1(R_0) \cap F^2(R_0)$.

CHAPTER 3

THE EXPONENTIALLY SELF-REGULATING MODEL

This chapter is organized as follows: In Section 3.1, we discuss some properties of the one-dimensional Exponentially Self-Regulating (hereafter, ESR) model. Next, in Section 3.2, we focus our discussion on the two-dimensional ESR model. We describe first the continuous form of the ESR dynamical system in the plane and then the associated discrete version (the ESR map) that is the subject of our investigation. Also, we discuss some normal forms of the planar ESR dynamical system that can be obtained using topological conjugacies (coordinate transformations). Then, in Section 3.3, we analyze several basic features of the two-dimensional ESR map including the location and types of its fixed points. As in the case of the LV map, we follow this in Section 3.4 with a brief description of a special uncoupled case of the ESR equations whose dynamics are determined primarily by those of the one-dimensional ESR map. We depict some aspects of the dynamics of a simple coupled case of the ESR equations in Section 3.5. We then prove in Section 3.6 that for certain ranges of the ESR map parameters, there is a chaotic regime generated by an orientation-reversing horseshoe map that we dub a *twisted horseshoe* with a *bending tail.* Furthermore, it is shown that the compact invariant set corresponding to the twisted horseshoe with bending tail is almost globally attracting — indicating that this population state is stable.

3.1 One-dimensional ESR Model

The discrete version of the one-dimensional ESR model for a single population is

$$x_{n+1} = ax_n e^{-bx_n}, \tag{3.1}$$

where $a, b > 0$. This actually has just one fundamental parameter, for the scaling $y_n = bx_n$ converts (3.1) (via a conjugacy) to

$$y_{n+1} = ay_n e^{-y_n}. \tag{3.2}$$

It is straightforward to prove that (3.2) exhibits essentially the same qualitative parameter-dependent dynamical behavior as the logistic model. We illustrate this briefly in the following few paragraphs.

The iterations in the difference equation (3.2) are generated by the function

$$g_a(y) = aye^{-y}. \tag{3.3}$$

Here, we take $a > 0$ so that a population that is initially positive remains positive.

In order to solve for the location of the fixed points of (3.3), we set

$$aye^{-y} = y,$$

and obtain two fixed points:

$$y_0 = 0 \quad \text{and} \quad y_1 = \ln a. \tag{3.4}$$

Thus $y = 0$ is the only realistic fixed point unless $a > 1$. If $0 < a \leq 1$, it is easy to show that $y = 0$ is a global attractor on the interval $[0, \infty)$, and so the dynamics are rather uninteresting. Therefore we shall assume that $a > 1$.

Before examining the types of the fixed points, we compute the derivative of $g_a(y)$:

$$g_a'(y) = a(1 - y)e^{-y}.$$

Now we determine the stability at the two possible fixed points.

The derivative at y_0 is

$$g_a'(y_0) = a,$$

so y_0 is a repelling fixed point since $a > 1$.

The derivative at y_1 is

$$g_a'(y_1) = 1 - \ln a,$$

so y_1 is an attracting fixed point if $1 < a < e^2$, a repelling fixed point if $e^2 < a$, and is degenerate if $a = e^2$. Figure 3.1 shows the first 200 forward iterations of $g_a(y)$ with an initial value, $y_0 = 2$. It is apparent that the one-dimensional ESR map exhibits dynamics similar to the logistic map, including the period-doubling route to chaos.

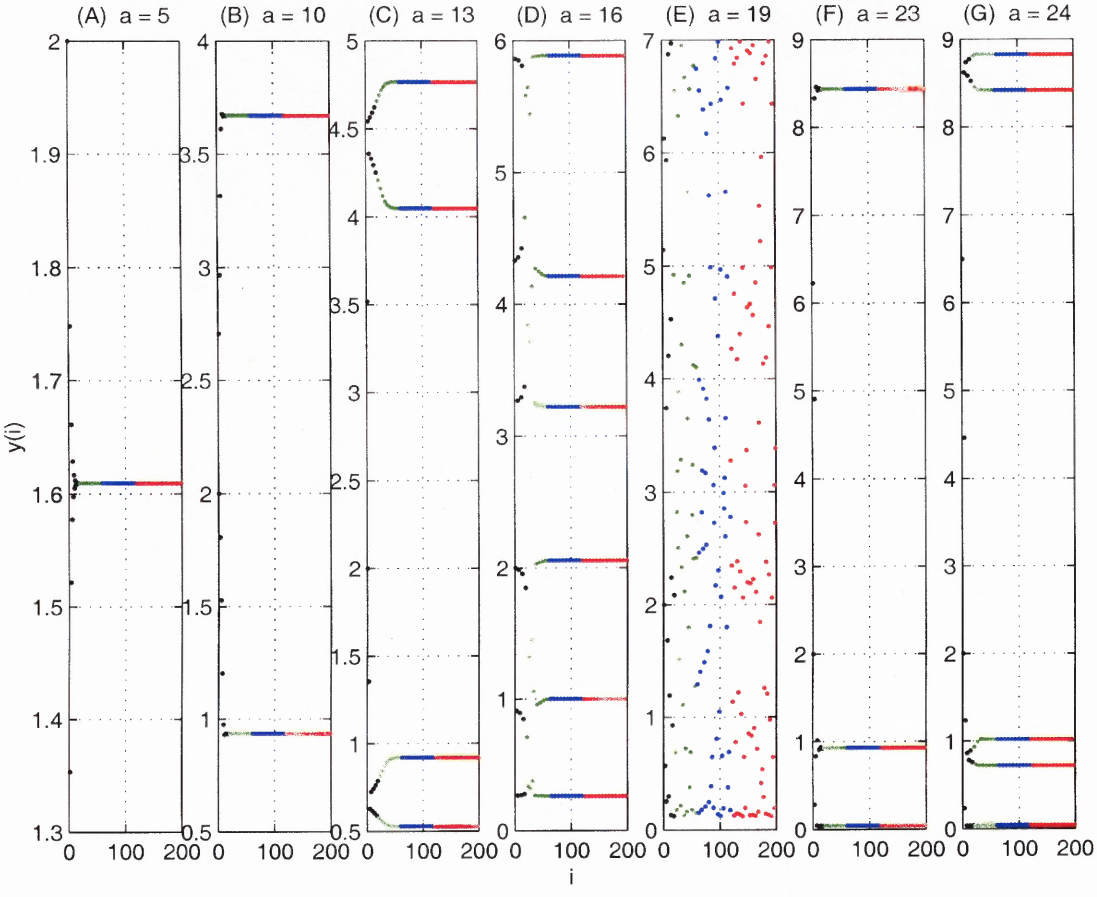

Figure 3.1 Dynamics of (3.3) for various values of a with $y_0 = 2$. We have in (A), steady state with $a = 5$; in (B), period-doubling bifurcation with $a = 10$; in (C), period four orbit with $a = 13$; in (D), period six orbit with $a = 16$; in (E), randomness with $a = 19$; in (F), period three orbit with $a = 23$; and in (G), period five orbit with $a = 24$.

The following table, showing the various dynamics of $g_a(y)$ with $1 < a < 100, a \in \mathbf{Z}^+$, makes it easier to predict the dynamics of the one-dimensional ESR map.

Type of Dynamics	a
Steady State	2—7
Period-Doubling	8—12
Period Three Orbit	23, 66, 81, 97
Period Four Orbit	13, 14, 29, 37, 51
Period Five Orbit	24
Period Six Orbit	16
Randomness	15, 17—22, 25—28, 30—36, 38—50
(Chaos)	52—65, 67—80, 82—96, 98, 99

Table 3.1 Various dynamics of (3.3) with $y_0 = 2$ and $1 < a < 100, a \in \mathbf{Z}^+$.

Next, we will discuss the one-hump dynamics associated with (3.3) for $y \geq 0$. It should be noticed that the one-dimensional ESR equation has an exponential factor, e^{-y}, that plays a dominant role in the dynamics for large values of y. The graph of the one-dimensional ESR map has one intersection point with the x-axis at the origin and looks like a concave-down parabola with an endless tail approaching the x-axis as $x \to \infty$. In Figure 3.2, periodic points are dotted in red, except in (E) that shows the one-hump dynamics which has the maximum height of $\frac{a}{e}$ at $y = 1$. We provide more figures with other values of a for the one-hump dynamics in Figure 3.3.

3.2 Two-dimensional ESR Model

It is not difficult to show the two-dimensional system of differential equations

$$\begin{aligned} \frac{dx}{dt} &= \lambda x e^{-ax-by}, \\ \frac{dy}{dt} &= \mu y e^{-cx-dy}, \end{aligned} \tag{3.5}$$

exhibits phase plane behavior similar to the two-dimensional Lotka-Volterra differential equations. Here, $\lambda, \mu > 0$ and the parameters $a, b, c, d \geq 0$ and $a+b+c+d > 0$ so as to avoid the trivial case where (3.5) is linear. In analogy with the association of the logistic map to the logistic differential equation, we define the (n-dimensional) Exponentially Self-Regulating (ESR) map to be the real analytic function $G : \mathbf{R}^n \to$

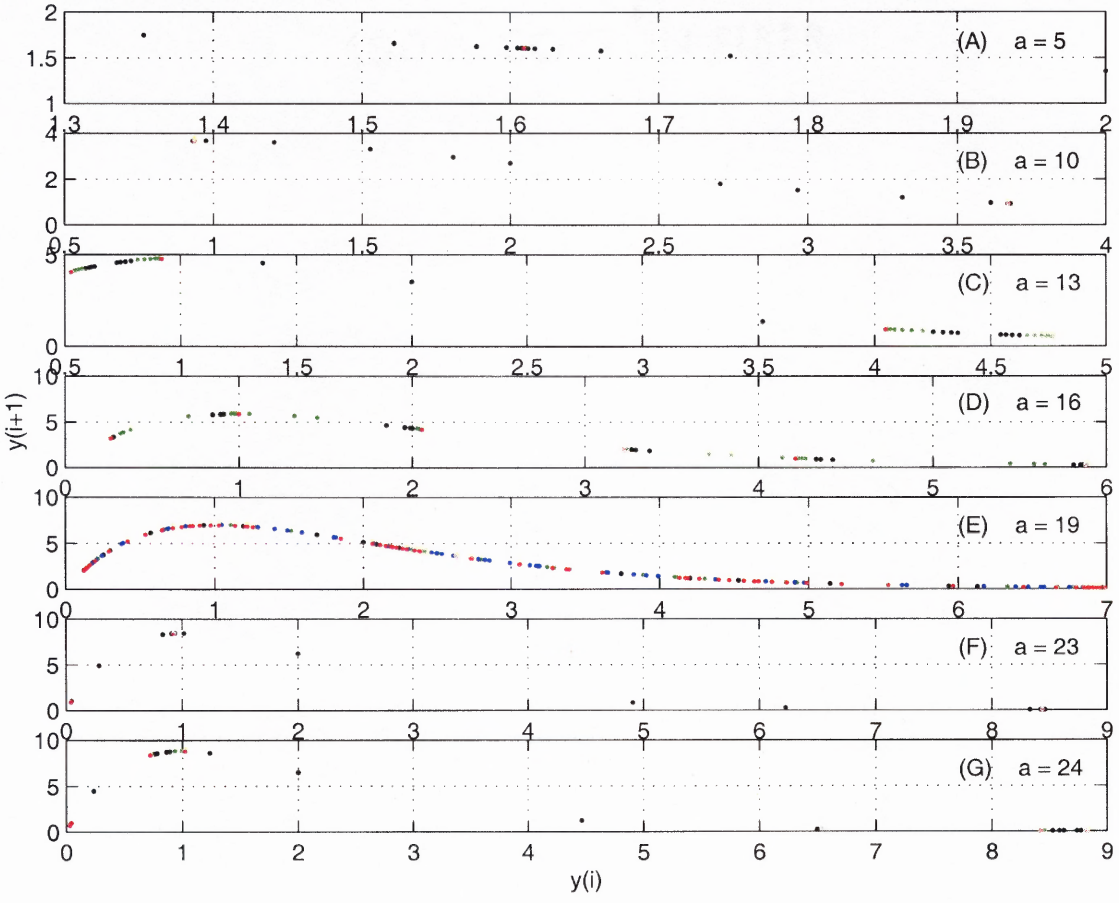

Figure 3.2 Periodicity of (3.3) for various values of a. In (A), the steady state with $a = 5$; in (B), period-doubling bifurcation with $a = 10$; in (C), period four orbit with $a = 13$; in (D), period six orbit with $a = 16$; in (E), randomness with $a = 19$; in (F), period three orbit with $a = 23$; and in (G), period five orbit with $a = 24$.

$\mathbf{R}^n$ defined by

$$G(\mathbf{x}) := A(\mathbf{x})\mathbf{x},$$

where $A(\mathbf{x})$ is an $n \times n$ real matrix function with entries of the form

$$a_{ij}(\mathbf{x}) = \alpha_{ij} exp\left(-\beta_{ij}^{(1)} x_1 - \beta_{ij}^{(2)} x_2 - \ldots - \beta_{ij}^{(n)} x_n\right), \quad (1 \leq i, j \leq n)$$

with $\alpha_{ij}, \beta_{ij}^{(1)}, \ldots, \beta_{ij}^{(n)} \geq 0$, satisfying the property that there exist an integer $k \geq 0$ and a positive constant σ such that

$$\|\mathbf{x}_{n+k+1}\| \leq \sigma \|\mathbf{x}_n\| e^{-\|\mathbf{x}_n\|}$$

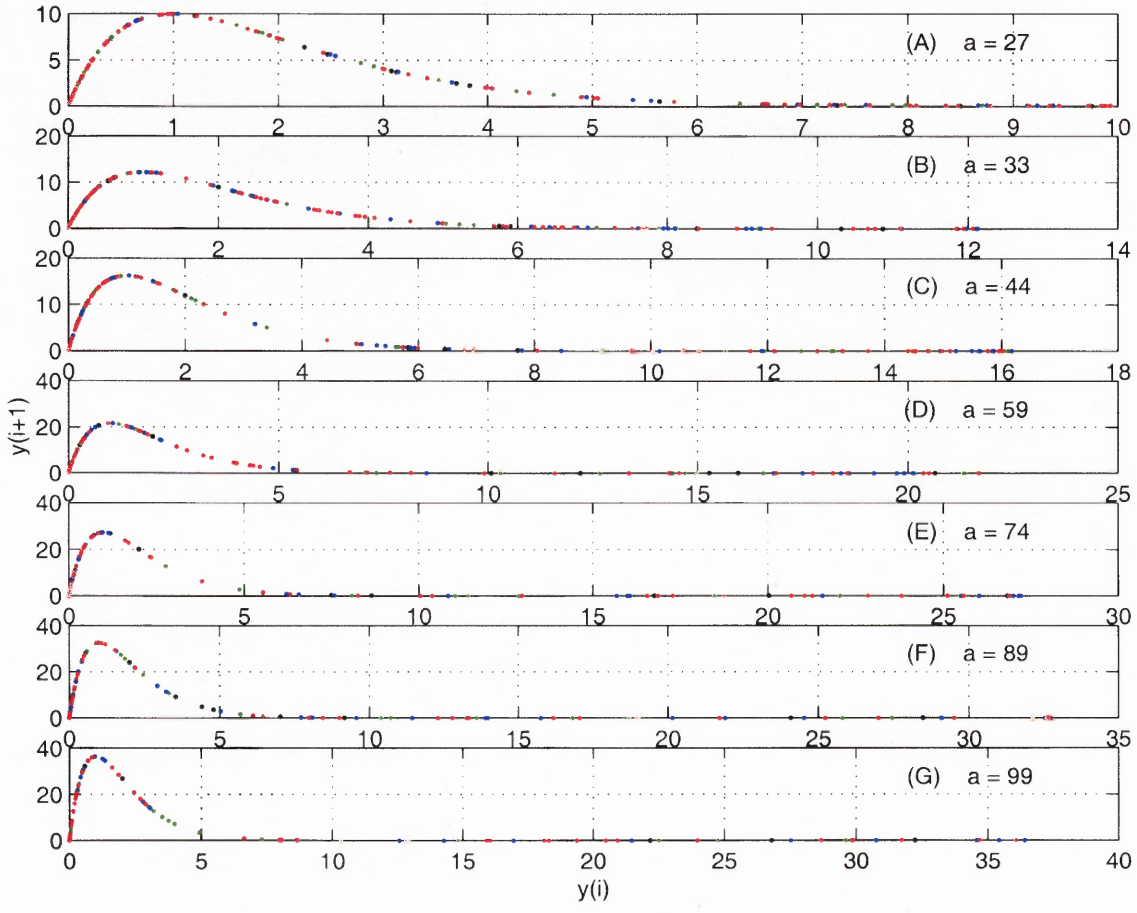

Figure 3.3 One-hump dynamics with various values of a. In (A), $a = 27$; in (B), $a = 33$; in (C), $a = 44$; in (D), $a = 59$; in (E), $a = 74$; in (F), $a = 89$; and in (G), $a = 99$.

for all $n \geq 0$, where $\mathbf{x}_{n+1} = G(\mathbf{x}_n)$ for all $n \geq 0$. Several studies have shown that discrete ESR models can accurately predict the dynamics of some actual populations (see, e.g. [50]).

We shall confine our attention to discrete ESR models for a pair of species and, in the interest of concreteness, further restrict our investigation to diagonal ESR maps of the form

$$G(x, y) := (\lambda x e^{-ax-by}, \mu y e^{-cx-dy}), \tag{3.6}$$

where the six parameters are subject to the same conditions as in (3.5). Note that G depends on the parameters $\Psi := (\lambda, \mu, a, b, c, d)$ and should therefore be denoted by G_Ψ. In some cases in the sequel we shall explicitly denote this parameter dependence, but in most cases, we shall simply maintain our slight and essentially harmless abuse of notation.

In certain cases the ESR map can be recast in simpler (normal) forms that actually reduce the number of parameters. For example, when both a and d are positive, (3.6) is topologically conjugate to

$$G_0(x, y) := (\lambda x e^{-x-\alpha y}, \mu y e^{-\beta x - y}), \tag{3.7}$$

with $\lambda, \mu > 0$ and $\alpha, \beta \geq 0$ via the conjugacy $\psi : \mathbf{R}^2 \to \mathbf{R}^2$ defined by

$$\psi(x, y) := (ax, dy).$$

On the other hand, with $\lambda, \mu > 0$, if $a = d = 0$ and $b, c > 0$, (3.6) is conjugate to

$$G_1(x, y) := (\lambda x e^{-y}, \mu y e^{-x}) \tag{3.8}$$

via the topological conjugacy $\psi(x, y) := (cx, by)$. We remark here that we have made obvious definitions or re-definitions of the parameters in the above normal forms. There are clearly other normal forms for other parameter choices, but we shall not consider them in the sequel. In particular, we shall investigate only (3.7) and (3.8), with comparatively little space being devoted to (3.8).

3.3 Analytical Results of the ESR Model

In this section, we shall express concisely the analytical results concerning the location and types of the fixed points of G as in the case of the LV model.

3.3.1 Location of Fixed Points

First, let us find those points where G does not have a local inverse; namely, the singular or critical points. So, we locate the zeros of the determinant of the derivative

of G, G', by computing

$$detG'(X) = \lambda\mu \begin{vmatrix} (1-ax)e^{-ax-by} & -bxe^{-ax-by} \\ -cye^{-cx-dy} & (1-dy)e^{-cx-dy} \end{vmatrix} = 0.$$

which leads to the following conic of singular points:

$$ax + dy - (ad - bc)xy = 1. \tag{3.9}$$

Then we determine the location and types of the fixed points of G. These points $X = (x, y)$ are solutions of the equations

$$\begin{aligned} \lambda x e^{-ax-by} &= x, \\ \mu y e^{-cx-dy} &= y, \end{aligned}$$

which give the following four fixed points:

$$\begin{gathered} X_0 = (0,0), \quad X_1 = (\tfrac{\ln\lambda}{a}, 0), \quad X_2 = (0, \tfrac{\ln\mu}{d}) \text{ and} \\ X_3 = \left(\tfrac{d\ln\lambda - b\ln\mu}{ad-bc}, \tfrac{a\ln\mu - c\ln\lambda}{ad-bc}\right), \end{gathered} \tag{3.10}$$

wherever the formulas make sense. We are only interested in the dynamics in the first quadrant of the plane. Note that X_1 and X_2 are in the first quadrant only if $\lambda > 1$ and $\mu > 1$, respectively, and X_3 is in the first quadrant only if $ad - bc$, $d\ln\lambda - b\ln\mu$ and $a\ln\mu - c\ln\lambda$ all have the same sign.

3.3.2 Stability Analysis

Here we determine the types of fixed points of G. The derivative at X_0 is

$$G'(X_0) = \begin{bmatrix} \lambda & 0 \\ 0 & \mu \end{bmatrix},$$

so X_0 is a source when $\lambda, \mu > 1$. If the fixed point X_1 exists, we compute that

$$G'(X_1) = \begin{bmatrix} 1 - \ln\lambda & -\frac{b\ln\lambda}{a}\lambda^{1-\frac{c}{a}} \\ 0 & \mu\lambda^{-\frac{c}{a}} \end{bmatrix},$$

with eigenvalues $1 - \ln\lambda$ and $\mu\lambda^{-\frac{c}{a}}$. So, for example, this is a (orientation-reversing) source if $\lambda > e^2$ and $\mu > \lambda^{\frac{c}{d}}$. At the fixed point X_2, we find that

$$G'(X_2) = \begin{bmatrix} \lambda\mu^{-\frac{b}{d}} & 0 \\ -\frac{c\ln\mu}{d}\mu^{1-\frac{b}{d}} & 1 - \ln\mu \end{bmatrix},$$

with eigenvalues $\lambda\mu^{-\frac{b}{d}}$ and $1 - \ln\mu$. For example, if $\mu > e^2$ and $\lambda < \mu^{\frac{b}{d}}$, then X_2 is a (orientation-reversing) saddle. Finally, we compute that the eigenvalues of $G'(X_3)$ are

$$\frac{1}{2}\left[D_+ \pm \sqrt{D_+^2 - 4D_\times}\right],$$

where

$$\begin{aligned} D_+ &:= \frac{ad(2 - \ln\lambda - \ln\mu) - 2bc + ab\ln\mu + cd\ln\lambda}{ad - bc}, \\ D_\times &:= 1 - ax_3 - dy_3 + (ad - bc)x_3y_3, \text{ and} \\ (x_3, y_3) &= X_3. \end{aligned}$$

We observe that both the x-axis and the y-axis are invariant manifolds for the discrete dynamical system of G. This is apparent for the forward iterations since if X has the first (second) coordinate equal to zero, then the same is true of $G(X)$. Observe that the restriction of G to either the x-axis or y-axis is basically the one-dimensional ESR map.

3.4 A Simple Uncoupled Case of the ESR Model

In this section we shall analyze some features of the special uncoupled case of the ESR map (3.7) with $\alpha = \beta = 0$; namely,

$$G(x, y) = (\lambda x e^{-x}, \mu y e^{-y}). \tag{3.11}$$

As the coordinates of G depend only on x and y, respectively, the dynamics is essentially one-dimensional. Note that G is just a product of one-dimensional ESR maps; i.e.,

$$G = g_\lambda \times g_\mu.$$

A few of the features of the iterations of this map are summarized below.

Since the ESR map is used as a population model, it makes sense to limit G to the first quadrant, Q_1, of the plane. When both $\lambda, \mu > 1$, it is obvious that the fixed

points of $G|_{Q_1}$ are $X_0 = (0,0)$, $X_1 = (\ln\lambda, 0)$, $X_2 = (0, \ln\mu)$ and $X_3 = (\ln\lambda, \ln\mu)$. When $\lambda, \mu > e^2$, all of the fixed points are repellers for the discrete dynamical system. In Figure 3.4, we illustrate the dynamics for $\lambda = 30$ and $\mu = 40$.

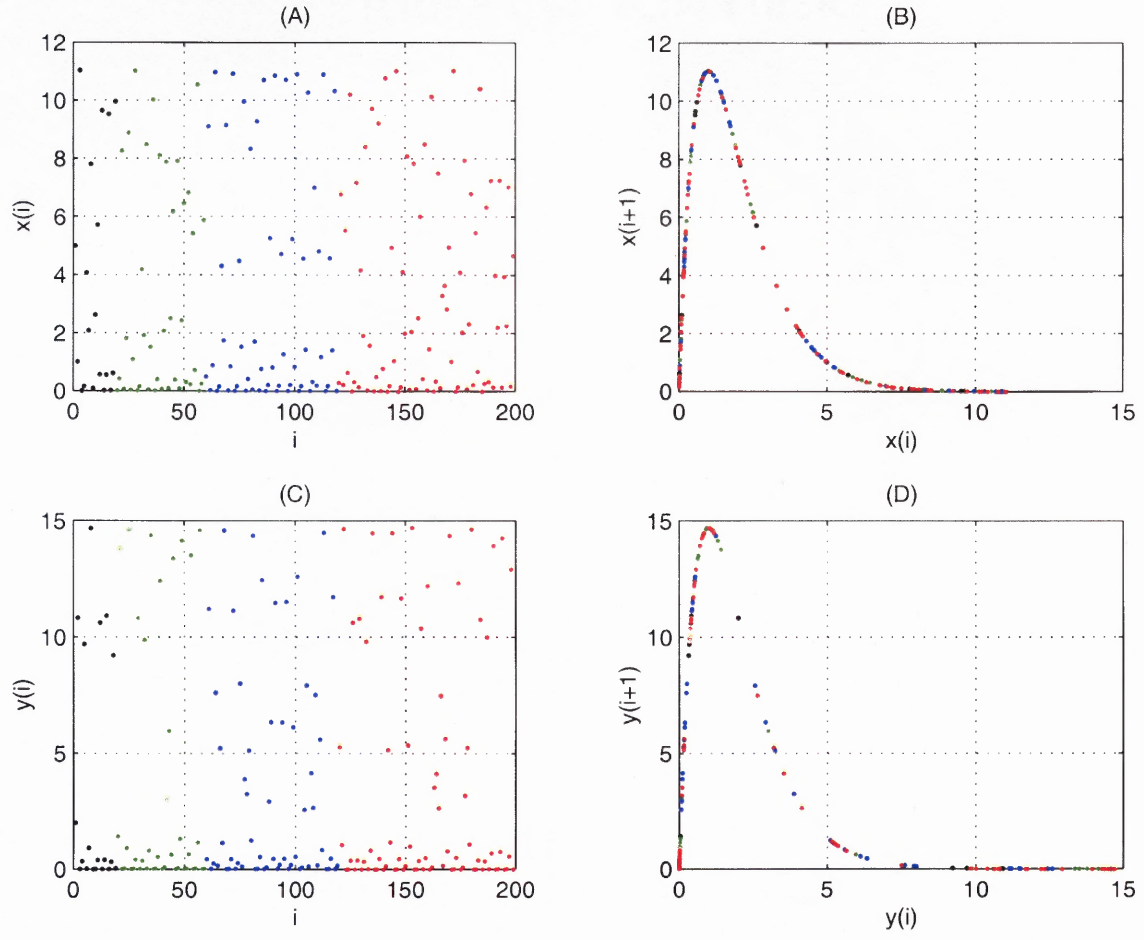

Figure 3.4 An uncoupled case of G with $\lambda = 30$ and $\mu = 40$ and initial values of $x_0 = 5$ and $y_0 = 2$. In (A) and (C), we plot the first 200 forward iterations for x_i and y_i, respectively; in (B) and (D), we plot the one-hump dynamics for x_i and y_i, respectively.

When $\lambda = \mu$, the map (3.11) also has the property of being symmetric with respect to the reflection $(x, y) \mapsto (y, x)$; i.e., this map is a conjugacy of G with itself. In addition to the x- and y-axes, G has the diagonal line $y = x$ as an invariant manifold and G restricted to the diagonal is a one-dimensional ESR map.

A basic fact can be drawn concerning (3.11): Although it subsumes the one-dimensional ESR map, its behavior is indeed totally determined by the dynamics of

the one-dimensional ESR map iterations. Accordingly, all of its dynamical properties can be readily obtained from those of the one-dimensional ESR map.

3.5 A Simple Coupled Case of the ESR Model

In this section we shall look into the dynamics of a simple, fully nonlinear, coupled special case of the ESR map given by (3.8); namely,

$$G(x, y) = (\lambda x e^{-y}, \mu y e^{-x}). \tag{3.12}$$

As we shall see, some interesting elements of the dynamical behavior of (3.12) are also basically logistic-like.

It is useful to begin with some observations. From the discussion in Section 3.3.1, the fixed points of the map defined by (3.12) are as follows: If both $\lambda, \mu > 1$, there are just two fixed points in Q_1 given by

$$X_0 = (0, 0), \quad X_3 = (\ln \mu, \ln \lambda); \tag{3.13}$$

if $0 < \lambda, \mu < 1$, X_0 is the only fixed point in Q_1; if $\lambda = 1$, $\mu \neq 1$, the whole x-axis consists of fixed points; and if both $\lambda, \mu = 1$, both the x- and y-axes are comprised of fixed points.

When $\lambda, \mu < 1$, the orbit structure for points in the first quadrant Q_1 is very simple.

Lemma 7 *If λ, $\mu < 1$, the first quadrant Q_1 is invariant with respect to the map G defined by (3.12). Furthermore, $(0, 0)$ is a global attractor for $G|_{Q_1}$.*

Proof: First we verify that $G(Q_1) \subset Q_1$. This is effortlessly done because $0 \leq x$, $0 \leq y$ implies that $0 \leq \lambda x e^{-y}$ and $0 \leq \mu y e^{-x}$ owing to the given hypothesis.

Then we note that $(0, 0)$ is the only fixed point of G in Q_1. A simple calculation shows that $G'(0)$ has eigenvalues λ and μ, so $(0, 0)$ is a sink. It is apparent from the

invariance of the x- and y-axes that positive semiorbits starting on the coordinate axes in Q_1 converge exponentially to $(0,0)$ with exponents λ and μ, respectively. The exponential convergence to $(0,0)$ of iterations of G starting in the interior of Q_1 can be directly inferred from the following inequality for $x^2+y^2>0$

$$\lambda^2x^2(e^{-y})^2+\mu^2y^2(e^{-x})^2<\lambda^2x^2+\mu^2y^2\leq\max\{\lambda^2,\mu^2\}(x^2+y^2).$$

So the proof is complete. □

We have a special symmetric case of (3.12) where logistic-like dynamics is the governing feature with the condition $\lambda=\mu$. In this instance, G is symmetric with respect to the reflection $(x,y)\to(y,x)$ in the sense that it is conjugate to itself via this isomorphism. The diagonal $y=x$ is an added invariant manifold for G, and the restriction of G to the diagonal is the one-dimensional ESR map $g:\mathbf{R}\to\mathbf{R}$ defined by

$$g_\lambda(x):=\lambda xe^{-x}.$$

Therefore as λ is changed, G undergoes the complete range of one-dimensional dynamics exhibited by the one-dimensional ESR map, including chaos and multiple periodic orbits. It is not difficult to verify in the symmetric case that the only interesting dynamical behavior results from one-dimensional ESR iterations.

A global description of the dynamics for the symmetric case is given in the following:

Lemma 8 *In (3.12), if $\lambda=\mu>1$, the dynamical system of iterations of G have the subsequent properties:*

(i) *G has exactly two fixed points: a source at $(0,0)$ and a fixed point at $(\ln\lambda,\ln\lambda)$ that bifurcates from a saddle into a source at $\lambda=e^2$.*

(ii) *G has exactly three linear, codimension-one, invariant manifolds: the x-axis, the y-axis and the diagonal $y=x$. G restricted to both the x- and y-axes is*

an expanding linear map of the form $x \to \lambda x$, while the restriction of G to the diagonal is the one-dimensional ESR map $g_\lambda(x) = \lambda x e^{-x}$.

(iii) *The dynamics of G exhibits chaos and multiple period orbits of a one-dimensional ESR map along the diagonal as λ is increased.*

Proof: Property (i) is an immediate result from the analysis shown in Section 3.3.1. The three manifolds in Property (ii) are in fact the only G-invariant, one-dimensional linear manifolds in the first quadrant as can readily be seen by tracking the iterations of points not on these lines. Along the diagonal, $y = x$, we have the one-dimensional ESR map $g : \mathbf{R} \to \mathbf{R}$ defined by

$$g_\lambda(x) := \lambda x e^{-x},$$

and it exhibits chaos and multiple period orbits of the one-dimensional ESR map as λ increases. This ends the proof. □

The proof of the following result can readily be obtained by making the rather obvious modification of the proof of Lemma 4 of Section 2.5.

Lemma 9 *If the ESR map (3.12) satisfies $\lambda, \mu > 1$ and $0 < \ln\lambda \ln\mu < 4$, then the following properties obtain:*

(i) *G has exactly two fixed points: a source at $X_0 = (0,0)$ and a saddle point $X_3 = (\ln\mu, \ln\lambda)$ in Q_1 and G has no other periodic points in Q_1.*

(ii) *The stable manifold V^s for the point X_3 is a smooth, open 1-dimensional submanifold of $\boldsymbol{R}^2$ contained in int Q_1, but not in any compact subset of Q_1, and its closure contains the additional point $X = (0,0)$.*

(iii) *The unstable manifold V^u for the point X_3 is a smooth, open one-dimensional submanifold of $\boldsymbol{R}^2$ that is unbounded, and eventually exits any square of the form $[0,a] \times [0,a]$, $a > \max\{\ln\lambda, \ln\mu\}$, at points on the upper and right edges and then never returns to the square.*

(iv) *The iterations of any point in* $Q_1 \backslash (\overline{V}^s \cup V^u)$ *under* G *eventually depart from any square of the form* $[0, a] \times [0, a]$, $a > 0$, *through its upper or right edge.*

The rather tame dynamical behavior described in Lemma 9 is portrayed in Figure 3.5 for the case $\lambda = 2, \mu = 12$.

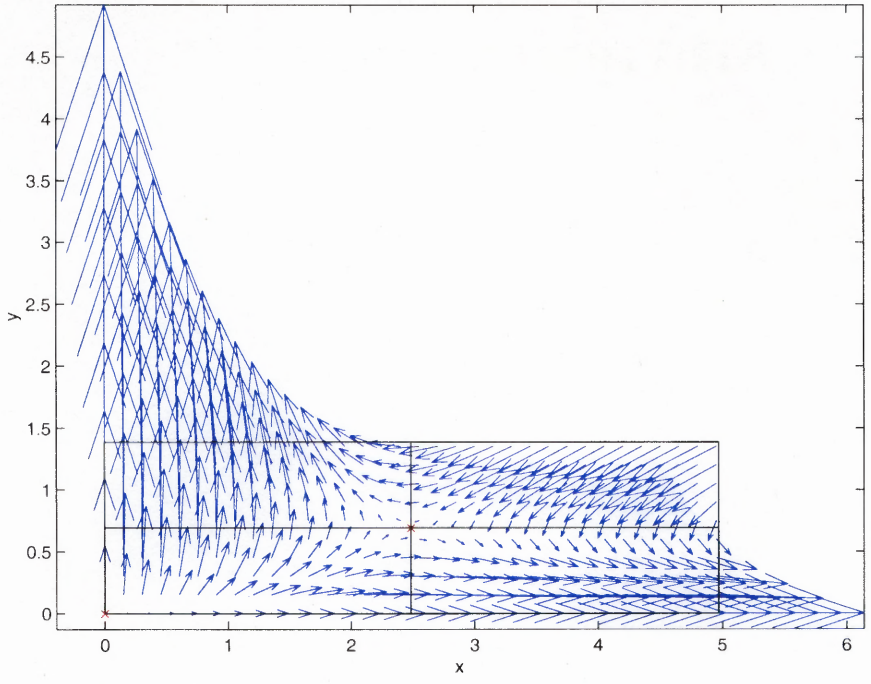

Figure 3.5 Dynamics of (3.12) for $\lambda = 2, \mu = 12$. The fixed points are $(0, 0)$ and $(2.4849, 0.6931)$ in two red 'x'-marks with eigenvalues $(2, 12)$ and $(2.3124, -0.3124)$, respectively.

We end this section with a conjecture about the dynamics of G when $(\ln \lambda)(\ln \mu) > 4$ in Lemma 9. It seems that the only intricate behavior in this case is of the variety of the one-dimensional ESR map.

Conjecture 10 *Suppose the ESR map (3.12) satisfies* $\lambda, \mu > 1$ *and* $(\ln \lambda)(\ln \mu) > 4$. *The dynamical properties are then as follows:*

(i) *The only fixed points of* G *are a source at the origin and a source at* $(\ln \mu, \ln \lambda)$.

(ii) *There exists a one-dimensional,* G*-invariant* C^1*-manifold of the form* $N = \{(x, \psi(x)) : \psi : \boldsymbol{R} \to \boldsymbol{R}\}$ *passing through the fixed points of* G *such that* ψ

is increased monotonously and the restriction $G|_N$ is a map that is conjugate to a one-dimensional ESR map. In particular, $G|_N$ has chaotic dynamics when $(\lambda + \mu)$ is large enough.

(iii) *The iterations of any point $X \subset Q_1 \backslash N$ converge to the x-axis or the y-axis.*

Part (i) of this conjecture is trivial (cf. the conjecture in Section 3.3.1). The critical part to prove is (ii), but if this can be done, it should be relatively simple to verify (iii). Figure 3.6 substantiates this conjecture for the case $\lambda = 20, \mu = 30$.

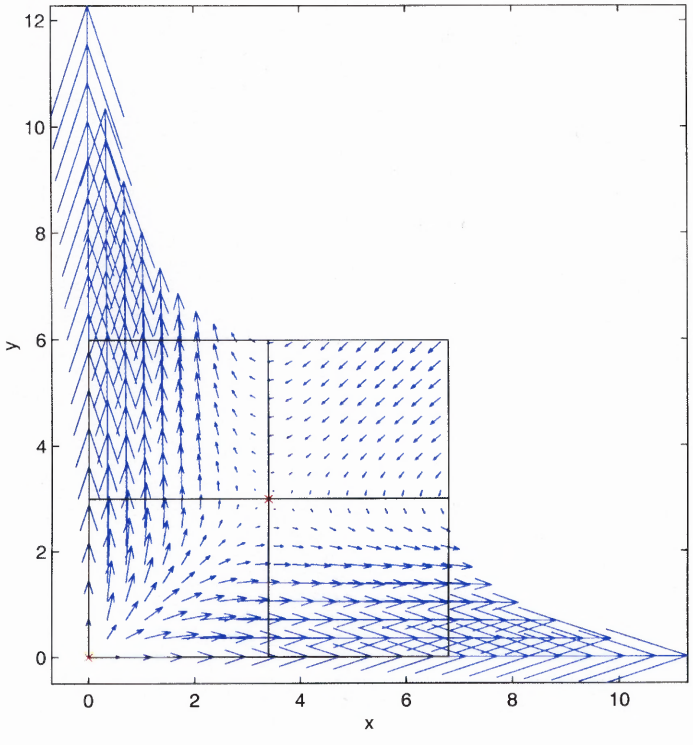

Figure 3.6 Dynamics of (3.12) for $\lambda = 20, \mu = 30$. The fixed points are $(0, 0)$ and $(3.4012, 2.9957)$ in two red 'x'-marks with eigenvalues $(20, 30)$ and $(4.192, -2.192)$, respectively.

3.6 A Particular Case of the ESR Model

Now we shall study the ESR map (3.7) more carefully, with an eye toward finding two-dimensional chaotic regimes similar to the twisted horseshoe dynamics exhibited

by the LV maps. The map to be studied is

$$G(x,y) := (\lambda x e^{-x-\alpha y}, \mu y e^{-\beta x - y}), \tag{3.14}$$

where the parameters α, β, λ and μ are all positive numbers. First we summarize some basic features of this map and its dynamics. The number and types of the fixed points of G depends on the parameters.

As expected, both the x-axis and y-axis are G-invariant and, as we shall describe in the sequel, G may have an added distinguished invariant set.

When $0 < \lambda, \mu \leq 1$, the positive semiorbits of G starting in Q_1 all converge to $(0,0)$ for all positive values of the parameters α and β. The restriction of G to the x- and y-axes are both one-dimensional ESR maps, so typical one-dimensional ESR map chaos and multiple period orbits occur along the coordinate axes as λ and μ are varied. It is simple to see that when $\lambda = \mu$ and $\alpha = \beta$, the diagonal $y = x$ is an added G-invariant set. The restriction of G to the diagonal in this case is the one-dimensional ESR map $x \mapsto \lambda x e^{-(\alpha+1)x}$, so it follows that G can have a one-dimensional chaotic regime distinct from those that may occur along the coordinate axes. So we see that the map (3.14) can show chaotic behaviors of the one-dimensional ESR type just like those of the simpler ESR maps that we considered in the Sections 3.4 and 3.5. Can it possibly be that (3.14) is capable of dynamical behavior that is chaotic in some kind of two-dimensional form essentially different from that of the one-dimensional ESR map? We shall attempt to answer this question in the affirmative in the sequel. As a matter of fact, we shall confirm the existence of a strange attractor for certain parameter ranges.

Our intention now is to define a rectangular region in Q_1 that is bounded below by the x-axis, has its remaining two sides vertical, contains the fixed point X_3 in its interior, and on which G acts like a (orientation-reversing) horseshoe map with a

bending tail. We denote this rectangular region by

$$R_1 := \{(x,y) : \ln\mu - a \le x \le \ln\mu + b,\ 0 \le y \le \rho\}, \text{ where}$$
$$0.05 \le a \le 0.1,\ b = \tfrac{a}{2} \text{ and } \rho \in \text{some constant.} \tag{3.15}$$

It is easy to verify that X_3 is in the interior of R_1. Of course, X_1 lies on the bottom edge of R_1 strictly between its endpoints (vertices).

The G-image of the bottom edge of R_1 is a small closed interval contained in the interior of the bottom edge, while the G-image of the top edge is a small, almost straight curve segment in the interior of R_1 that lies near and is almost parallel to the bottom edge of R_1 (see Figure 3.7).

Hence the G-images of the bottom edge and top edge of R_1 are two disjoint closed intervals in the interior of the bottom edge of R_1, with the image of the top edge of R_1 lying to the left of the image of the bottom edge of R_1 (see Figure 3.7).

The left and right edge image curves of R_1 exhibit the same orientation-reversing one-hump dynamics as the one-dimensional ESR map, and an example of this is shown in Figure 3.7. It can be shown that for the case under consideration, both of the image curves attain their maximum heights at points in Q_1 below the top edge of R_1. Moreover, these two curve segments have precisely one intersection point — a point that lies below the top edge of R_1. Consequently, we conclude that $G(R_1)$ is obtained from R_1 by squeezing (essentially in the horizontal direction), stretching (approximately in the vertical direction), applying a single twist and then folding over so that it intersects R_1 in two approximately vertical curvilinear rectangular regions as illustrated in Figure 3.7 and 3.8. Note that the bending tail atop the x-axis is a result of having a larger coefficient value of the exponential term of y in the second component of G. Hence, it is quite natural to refer to the restriction of G to R_1 as a *twisted horseshoe* with a *bending tail.*

Theorem 11 *For the range of parameters*

$$10^{-3} \le \alpha, \beta \le 10^{-2},\ \ 2.5 \le \lambda \le 3,\ \ 28 \le \mu \le 30,$$

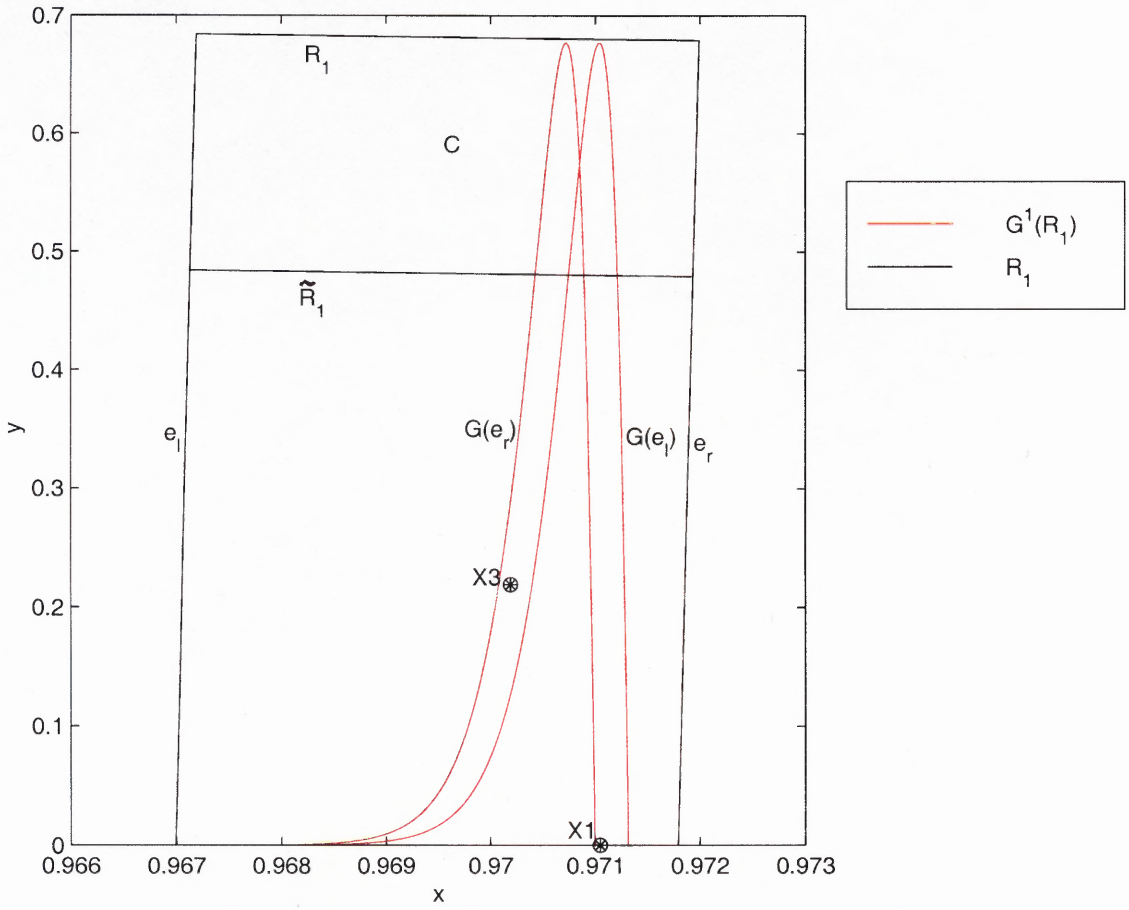

Figure 3.7 The action of G^1 on R_1 showing the twisted horseshoe with bending tail.

the ESR map

$$G(x, y) = \left(\lambda x e^{-x-\alpha y}, \mu y e^{-\beta x - y}\right)$$

exhibits chaotic dynamics on a compact strange attractor Λ *contained in the rectangle*

$$R_1 := \{(x, y) : \ln\lambda - 0.1 \leq x \leq \ln\lambda + 0.05,\ 0 \leq y \leq 0.7\}.$$

Λ *is the closure of the unstable manifold of the fixed point*

$$X_3 = \left(\frac{\ln\lambda - \alpha\ln\mu}{1-\alpha\beta}, \frac{\ln\mu - \beta\ln\lambda}{1-\alpha\beta}\right),$$

$G|_\Lambda$ *is conjugate to a subshift and the basin of attraction of* Λ *in the first quadrant is the whole first quadrant minus the* y*-axis.*

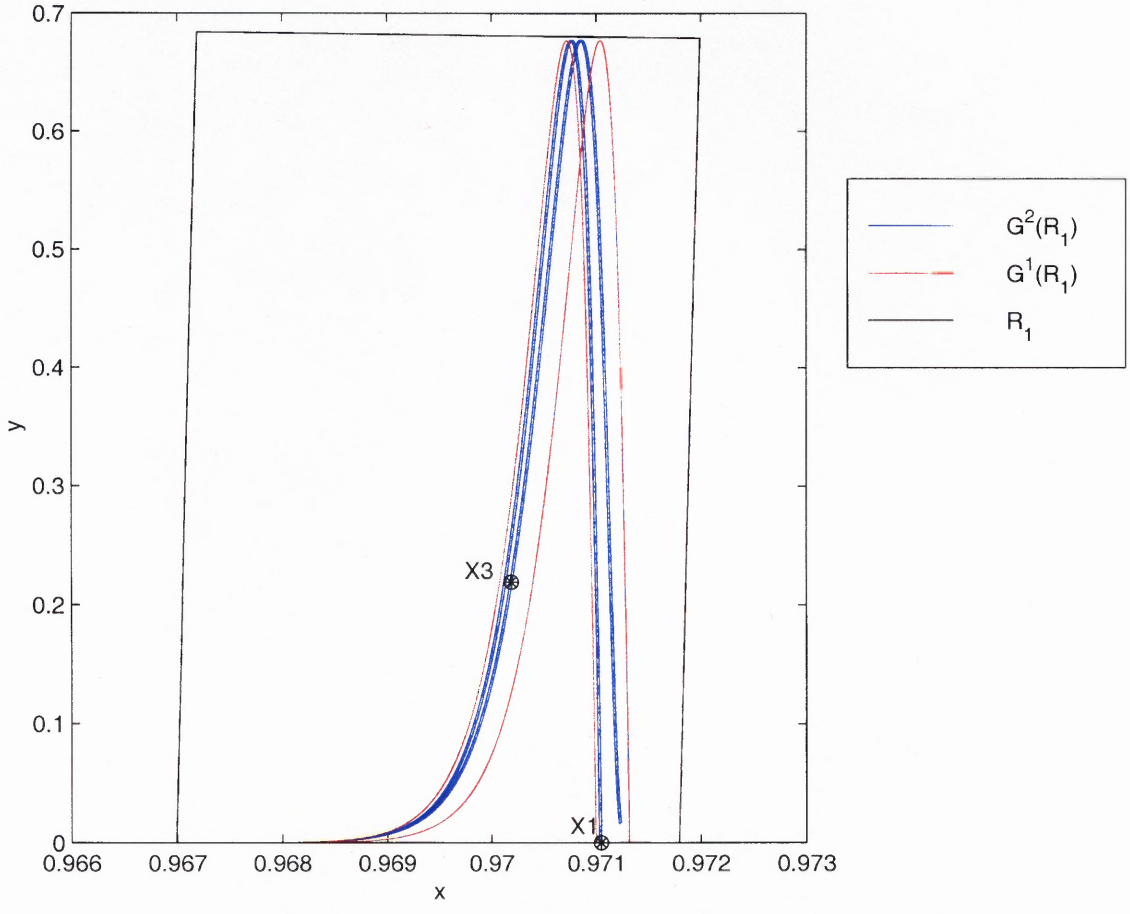

Figure 3.8 The action of G^2 and G^1 on R_1.

Proof: First we define the rectangle

$$\tilde{R}_1 := \{(x, y) : \ln \lambda - 0.1 \leq x \leq \ln \lambda + 0.05,\ 0 \leq y \leq 0.5\}.$$

and set C equal to the closure of $R_1 \backslash \tilde{R}_1$. Let e_l and e_r denote the left and right sides of the rectangle R_1, respectively. It is easy to show that for the specified parameter ranges G maps R_1 as shown in Figure 3.7. We call the mapping in R_1 a *twisted horseshoe with bending tail* and note that we can assume that G is a diffeomorphism on $G(\tilde{R}_1)$ with inverse obtained by choosing the proper branch of G^{-1} on R_1.

Obviously the set defined as

$$\Lambda := \bigcap_{n=0}^{\infty} G^n(R_1)$$

is a G-invariant set contained in R_1, and it is certainly compact. It is clear from the construction of Λ that it is just the closure of the unstable manifold of the fixed point X_3. We note also that Λ is a local attractor in the first quadrant inasmuch as it follows from its construction that the forward iterations under G of any point in R_1 converge to Λ. In fact, a closer inspection of G shows that forward iterations of any point in the first quadrant, except those on the y-axis, eventually wind up in R_1. Therefore we conclude that the basin of attraction of Λ in the first quadrant is

$$B(\Lambda) = \{(x, y) : 0 < x,\ 0 \leq y\}$$

To see that the dynamics of $G|_\Lambda$ are chaotic, we observe that it follows from the construction of Λ that it contains points of transverse intersection of the stable and unstable manifolds of the saddle point X_3. Consequently, by a theorem of Smale ([17], [51]), $G|_\Lambda$ is conjugate to a subshift (i.e., for some positive integer m, G^m is conjugate to the shift map on the space of doubly-infinite binary sequences). Hence Λ is a strange attractor (which is homeomorphic to the product of an interval and a two-component Cantor set) and $G|_\Lambda$ is chaotic. Thus the proof is complete. □

By interchanging λ and μ and α and β in (3.14), we note that it is feasible to create a twisted horseshoe with bending tail behavior for G in a rectangular region bounded by a line segment on the positive y-axis instead of the positive x-axis. The parameter values used in drawing Figures 3.7 and 3.8 are as followed: $\alpha = 0.0043$, $\beta = 0.048$, $\lambda = 2.91$ and $\mu = 29.3$.

Here we provide a couple more figures showing forward iterations of randomly selected points. In Figure 3.9, all 1000 points are selected randomly within R_1, and their first three forward iterations are shown with different colors. In Figure 3.10, a random point, G^0, is chosen within R_1 and its first 500 forward iterations, $G^1, G^2, \ldots, G^n$, are plotted as shown.

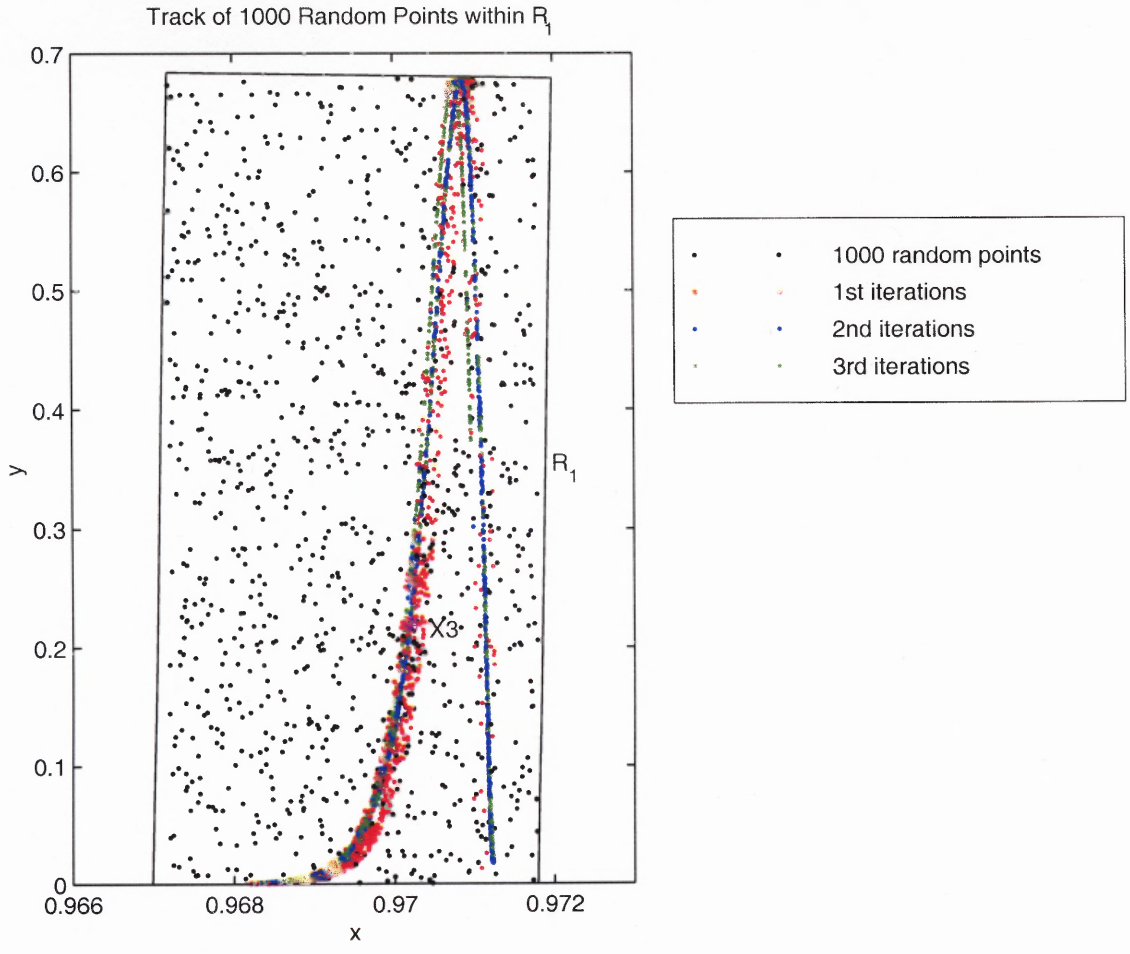

Figure 3.9 Randomly selected 1000 points' iterations within R_1: first 3 forward iterations.

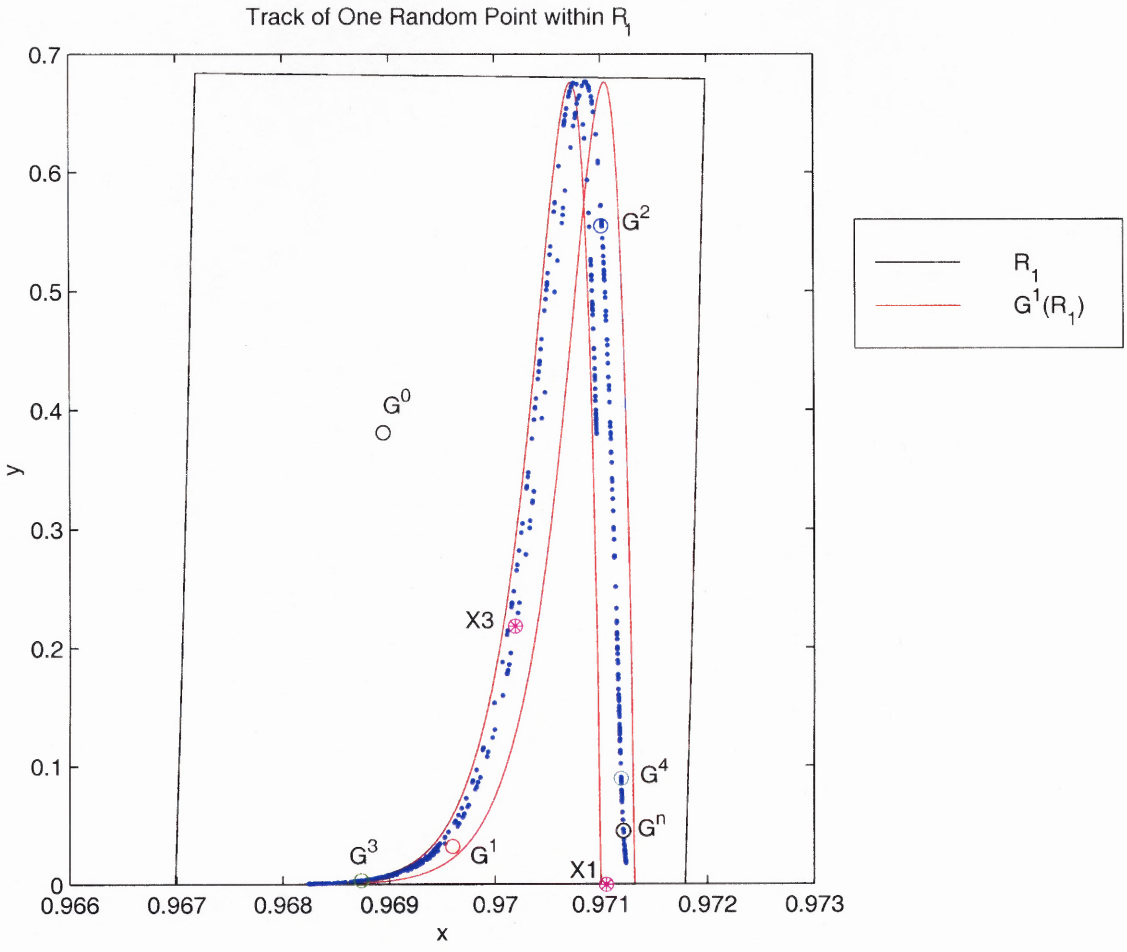

Figure 3.10 The track of one random point: first 500 iterations of G.

CHAPTER 4
DISCUSSION, CONCLUSIONS AND FUTURE WORK

In Section 4.1, we will discuss the similarities and differences between the LV model studied in Section 2.6 and the ESR model investigated in Section 3.6. Then, in Section 4.2, we draw conclusions on each of the models discussed. In the end, we describe some possible directions for future work in Section 4.3.

4.1 Discussion

In Chapters 2 and 3, we have investigated the LV model and the ESR model, respectively, using a combination of analytical and numerical techniques. It is now our intention to look into their similarities and differences and to discuss some inferences that can be made from a careful comparison of these two discrete population models.

4.1.1 Similarities between the LV and ESR Models

Within physically reasonable parameter values, both (2.11) and (3.14) may have as many as four distinct fixed points, and by choosing the ranges of parameter values correctly, we can force the fourth fixed point (lying in the interior of the first quadrant) to be a saddle point. For certain parameter ranges, the dynamics of the LV map is essentially that of the logistic map and the dynamics of the ESR map is essentially that of the one-dimensional ESR map, and the dynamics of both one-dimensional maps are qualitatively the same. If we expand the right hand side of (3.14) in a Taylor series, we find that

$$\begin{aligned} \lambda x e^{-x-\alpha y} &\simeq \lambda x\left[1+(-x-\alpha y)+\tfrac{(-x-\alpha y)^2}{2!}+\tfrac{(-x-\alpha y)^3}{3!}+\cdots\right] \\ &\simeq \lambda x\left[1-(x+\alpha y)+\tfrac{(x+\alpha y)^2}{2!}-\tfrac{(x+\alpha y)^3}{3!}+\cdots\right] \quad \text{and} \\ \mu y e^{-\beta x-y} &\simeq \mu y\left[1+(-\beta x-y)+\tfrac{(-\beta x-y)^2}{2!}+\tfrac{(-\beta x-y)^3}{3!}+\cdots\right] \\ &\simeq \mu y\left[1-(\beta x+y)+\tfrac{(\beta x+y)^2}{2!}-\tfrac{(\beta x+y)^3}{3!}+\cdots\right]. \end{aligned} \tag{4.1}$$

Then if we discard the higher order terms in the expansions above, we see that

$$\begin{aligned} \lambda x e^{-x-\alpha y} &\approx \lambda x[1-(x+\alpha y)] = \lambda x(1-x-\alpha y) \quad \text{and} \\ \mu y e^{-\beta x-y} &\approx \mu y[1-(\beta x+y)] = \mu y(1-\beta x-y) \end{aligned} \tag{4.2}$$

which is just the same as the right hand side of (2.11). Thus we see that the LV map approximates the ESR map up to quadratic terms. If we take more terms in the expansion of (4.1), for example,

$$\begin{aligned} \lambda x e^{-x-\alpha y} &\approx \lambda x[1-(x+\alpha y)+\tfrac{(x+\alpha y)^2}{2!}-\tfrac{(x+\alpha y)^3}{3!}] \quad \text{and} \\ \mu y e^{-\beta x-y} &\approx \mu y[1-(\beta x+y)+\tfrac{(\beta x+y)^2}{2!}-\tfrac{(\beta x+y)^3}{3!}], \end{aligned}$$

it is likely that the dynamical behavior of the map on the right should more closely approximate that of the ESR map, but more work needs to be done to confirm this.

4.1.2 Differences between the LV and ESR Models

An obvious difference between the LV and ESR models is that one of the species in the LV map may vanish (become extinct) over time, while in the ESR model neither of the two species can become extinct, although each of the populations can become extremely small. This difference can be linked with the lack of higher order terms in the LV map described above.

Another important dissimilarity in the dynamics of these two maps concerns the nature of their chaotic regimes: The twisted horseshoe dynamics of the LV map is associated with a Cantor-like invariant set that repels all nearby points except those in a subset of measure zero, while the chaotic dynamics of the ESR map essentially occurs on a Cantor-like strange attractor that attracts all points in the first quadrant except those on one coordinate axis.

4.1.3 Comparison of LV and ESR Models

At the end of Chapter 2, we showed three tables of forward iterations of points for the LV map, where six types of locations of initial points were chosen randomly. It

has been shown that the invariant set corresponding to chaotic LV dynamics,

$$\bigcap_{n\in\mathbf{Z}^+} \Lambda_{\pm n} := \bigcap_{n\in\mathbf{Z}^+} \{F^{\pm n}(\Lambda_0) \cap \Lambda_0 : n \in \mathbf{Z}^+\}, \tag{4.3}$$

repels almost all nearby points. Here, we present a similar compilation of iterations for the ESR map which shows the attracting property for randomly selected initial points in the first quadrant. Figure 4.1 illustrates four types of locations of the randomly selected initial points, G^0, and their first 1000 forward iterations, $G^1, G^2, \ldots, G^n$, generated by (3.14).

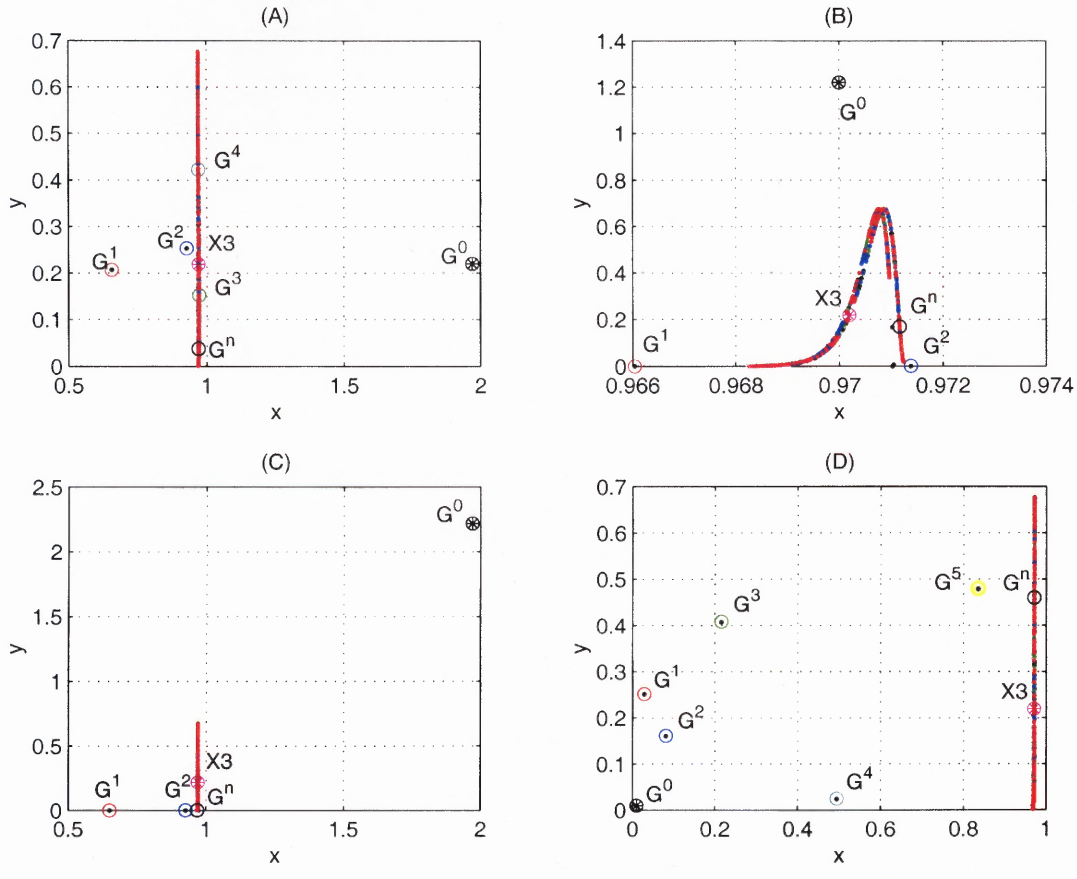

Figure 4.1 Four types of locations of randomly selected initial points and their first 1000 forward iterations. In (A), the initial point is one unit to the right of X_3; in (B), the initial point is one unit to the top of X_3; in (C), the initial point is one unit to the right and the top of X_3; and in (D), the initial point is at $(0.01, 0.01)$. The location of X_3 is $(0.9702, 0.2191)$.

It is harder to visualize the orbit of the forward iterations when the initial point is just one unit away from the saddle point than it is when the initial point

is chosen to be close to the saddle point X_3. To show this, in Figure 4.2, an initial point is chosen to be close to X_3 and within R_1 and its first 2000 forward iterations are shown.

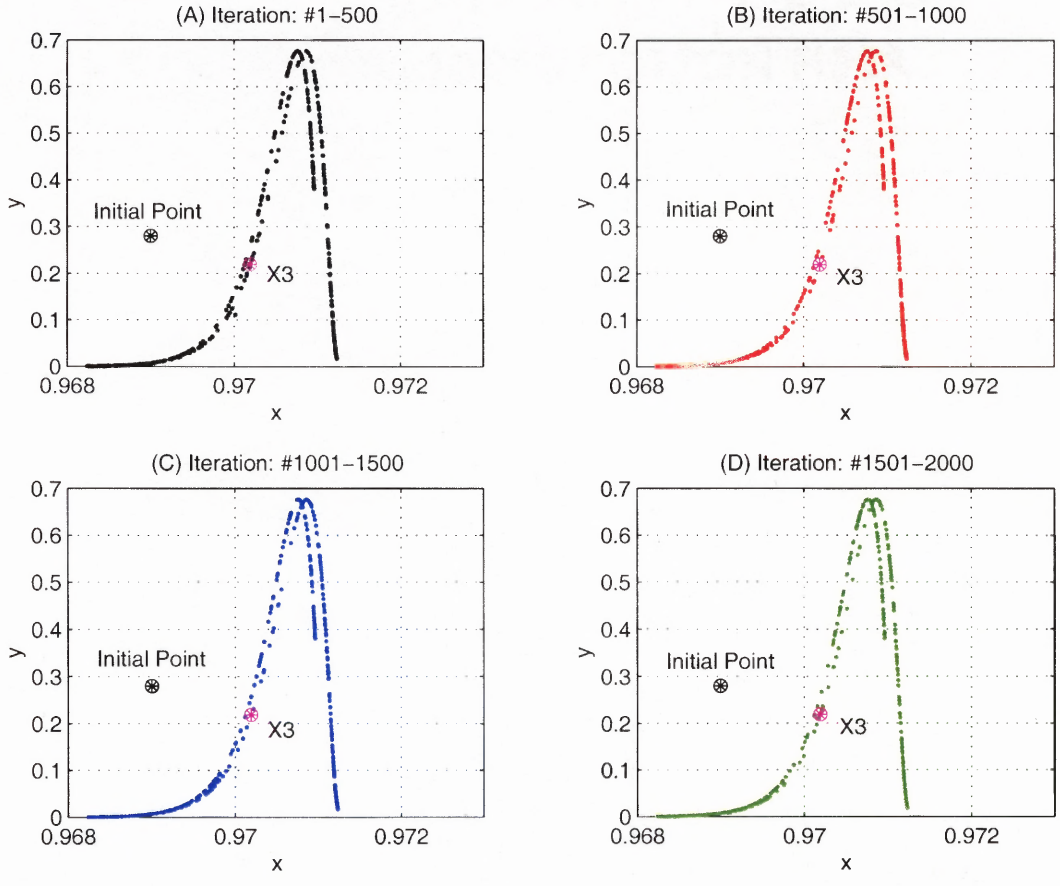

Figure 4.2 An initial point, $(0.969, 0.28)$, is chosen randomly within R_1 and its first 2000 forward iterations are depicted: in (A), iteration $\#1 - 500$; in (B), iteration $\#501 - 1000$; in (C), iteration $\#1001 - 1500$; and in (D), iteration $\#1501 - 2000$.

Now, it is easier to see the orbit of the forward iterations that exhibits the same structure of dynamics for each of the 500 forward iterations as shown in (A)-(D) of Figure 4.2.

4.2 Conclusions

In this dissertation we have introduced and proven the existence of twisted horseshoe and twisted horseshoe with bending tail chaos for the discrete LV and ESR models,

respectively. This has provided new insights into the surprising complexity of competing species dynamics. Our analysis has been extensive but not exhaustive, so there remain many open problems for future research. We should note that the seeming lack of relevant field data in the literature has prevented us from making the kinds of comparisons that would demonstrate the applicability of our models to actual populations. This is something that we plan to work on in the future.

We have undertaken quite an extensive analysis of the dynamics of both the two-dimensional discrete LV and ESR population models. Therefore, we are now in a position to make some significant concluding remarks about each of these models.

In Chapters 2 and 3, we introduced and analyzed discrete versions of the Lotka-Volterra (LV) and Exponentially Self-Regulating (ESR) differential equations as dynamical models for the interaction of two competing species. These choices of models are quite plausible for two-species systems: they certainly contain enough parameters to cover the important phenomenological features of most competing species scenarios. Moreover, they are quite natural in light of what we know about the effectiveness of using a discrete (difference) form of the logistic differential equation as a model for the evolution of a single species. Both the discrete LV and ESR systems produce, as one might expect from what is known about the comparative properties of the discrete and continuous logistic models and one-dimensional discrete ESR model, respectively, a far richer assemblage of dynamics than does the continuous model. For example, our analysis shows that both the two-dimensional discrete LV and ESR systems can exhibit period-doubling cascades leading to chaotic regimes that are essentially one-dimensional and something more — for certain parameter ranges, the discrete dynamics includes orientation-reversing horseshoe maps that we have dubbed twisted horseshoe and twisted horseshoe with bending tail maps. Hence, not only do the LV and ESR maps subsume all the dynamics of the one-dimensional discrete logistic model and the one-dimensional discrete ESR model, respectively,

they can generate a fully two-dimensional form of chaotic behavior. The chaotic regime is unstable for the LV map, bot almost globally attracting (stable) for the ESR map. This robustness of the chaotic regime for the ESR model renders it observable for actual populations.

Although we have in Chapters 2 and 3 undertaken a rather thorough investigation of the dynamics of the discrete LV and ESR models for a pair of competing species that has apparently revealed, at least in a qualitative sense, all of its possible dynamical features, our study has not been exhaustive. We have not obtained a complete breakdown of all the dynamic properties correlated with the entire domain of meaningful parameter values. It may in fact be too ambitious even to attempt such a complete correspondence between the parameter domain and range of dynamical behaviors. Nevertheless, it would certainly be useful to obtain more precise estimates of the parameter regions that support some of the more interesting and exotic dynamics — for example, twisted horseshoes and twisted horseshoes with bending tails — especially when it is possible to identify certain special cases of the discrete LV and ESR systems that can serve as useful predictive models for actual competing species in real environments.

Our last comment concerning the need for additional analysis of discrete LV and ESR systems that have demonstrable applications to population biology is especially pertinent. For it remains to identify meaningful examples of competing species systems to which the LV and ESR maps can be applied as a predictive tool in a way that compares favorably with the results of field data and simulation. If it is found that the LV or ESR maps do not work as effective models for a wide class of competing population scenarios, it would then be natural to ask what kind, if any, of minor modifications of the LV or ESR maps can produce a significant enlargement of the class of real problems in population biology to which they are applicable. It has already been shown that ESR models provide rather effective predictive capabilities

for a wide class of competing population scenarios ([49] and [50]). These and some related questions are something we plan to address more thoroughly in the near future.

4.3 Future Work

A more general version of the two-dimensional ESR model we studied can be written as

$$\begin{aligned} x_{n+1} &= \lambda_1 x_n e^{-\alpha_{11}x_n-\beta_{11}y_n} + \mu_1 y_n e^{-\alpha_{12}x_n-\beta_{12}y_n} \\ y_{n+1} &= \lambda_2 x_n e^{-\alpha_{21}x_n-\beta_{21}y_n} + \mu_2 y_n e^{-\alpha_{22}x_n-\beta_{22}y_n}. \end{aligned} \tag{4.4}$$

In (4.4), if we set the parameter values to be

$$\lambda_1 = \mu_2 = 0,\ \mu_1 = a,\ \lambda_2 = b,$$

$$\alpha_{12} = 0,\ \beta_{12} = \alpha_{21} = 1 \text{ and } \beta_{21} = \mu,$$

then, we obtain the following system of equations

$$\begin{aligned} x_{n+1} &= a y_n e^{-y_n} \\ y_{n+1} &= b x_n e^{-x_n-\mu y_n}, \end{aligned} \tag{4.5}$$

which is just the so-called pioneer-climax model studied by Nisbet and Onyiah ([49]). Although it would be more difficult to analyze the dynamics of (4.4) than it was for the diagonal ESR model investigated in this thesis, we suspect that the more general system has the same dynamical features as the diagonal system. This conjecture is certainly worthy of additional attention, and we may conduct a more thorough investigation of this matter in the future.

A three-dimensional version of the more general ESR model can be written as

$$\begin{aligned} x_{n+1} &= \lambda_1 x_n e^{-\alpha_{11}x_n-\beta_{11}y_n-\gamma_{11}z_n} + \mu_1 y_n e^{-\alpha_{12}x_n-\beta_{12}y_n-\gamma_{12}z_n} + \sigma_1 z_n e^{-\alpha_{13}x_n-\beta_{13}y_n-\gamma_{13}z_n} \\ y_{n+1} &= \lambda_2 x_n e^{-\alpha_{21}x_n-\beta_{21}y_n-\gamma_{21}z_n} + \mu_2 y_n e^{-\alpha_{22}x_n-\beta_{22}y_n-\gamma_{22}z_n} + \sigma_2 z_n e^{-\alpha_{23}x_n-\beta_{23}y_n-\gamma_{23}z_n} \\ z_{n+1} &= \lambda_3 x_n e^{-\alpha_{31}x_n-\beta_{31}y_n-\gamma_{31}z_n} + \mu_3 y_n e^{-\alpha_{32}x_n-\beta_{32}y_n-\gamma_{32}z_n} + \sigma_3 z_n e^{-\alpha_{33}x_n-\beta_{33}y_n-\gamma_{33}z_n}. \end{aligned} \tag{4.6}$$

In (4.6), if we set the parameter values to be

$$\lambda_1 = \mu_1 = 0,\ \sigma_1 = b,\ \alpha_{13} = c_{el},\ \beta_{13} = 0,\ \gamma_{13} = c_{ea},$$

$$\lambda_2 = 1 - \mu_l,\ \mu_2 = \sigma_2 = 0,\ \alpha_{21} = \beta_{21} = \gamma_{21} = 0,$$

$$\lambda_3 = 0,\ \mu_3 = 1 - \mu_p,\ \sigma_3 = 1 - \mu_a,\ \alpha_{32} = \beta_{32} = 0,\ \gamma_{32} = c_{pa},$$

$$\text{and } \alpha_{33} = \beta_{33} = \gamma_{33} = 0,$$

and replace (x_n, y_n, z_n) by (L_n, P_n, A_n), then, we obtain the following system of equations

$$\begin{aligned} L_{n+1} &= bA_n e^{-c_{el}L_n - c_{ea}A_n} \\ P_{n+1} &= (1-\mu_l)L_n \\ A_{n+1} &= (1-\mu_p)P_n e^{-c_{pa}A_n} + (1-\mu_a)A_n, \end{aligned} \tag{4.7}$$

which is the model investigated by Costantino et al. ([50]). This system was used to model the dynamical behavior of the flour beetle Tribolium, where L_n, P_n and A_n represent the larvae, pupae and adult populations at time n, respectively, of the total beetle population. The researchers found that for certain parameter values, the predictions of the dynamical model agreed very well with experimental field data collected from a selected Tribolium colony. We hope to find additional biological applications of our ESR models in our future research.

We plan to investigate a number of open questions concerning Lotka-Volterra (LV) models, Exponentially Self-Regulating (ESR) models and other related discrete dynamical system models that can be usefully applied in the study of population biology. It is our hope to collaborate with some population biologists in order to focus our attention on important and relevant problems arising in this field.

There are several possible directions for future research on the models we have studied in Chapters 2 and 3. To name a few, the two-dimensional prey-predator population model and the cooperation population model. Also, it is logical to examine three-dimensional and higher dimensional population models of all three

types of interactions between species. It should be interesting to see how well the LV and ESR models work for three or more types of interacting populations.

Returning to the field of two-dimensional models, recently, it has come to our attention that there is a model, rather closely related to both the LV and ESR models, that is actively being studied by both mathematical scientists and population biologists: Franke and Yakubu ([57]-[60]) and other researchers such as Namkoong and Selgrade ([61]) have studied the pioneer-climax model for two interacting species of the form

$$\begin{aligned} x_{n+1} &= x_n e^{a-x_n-y_n} \\ y_{n+1} &= y_n(x_n+y_n)e^{b-x_n-y_n}. \end{aligned} \tag{4.8}$$

It appears that the techniques that we have developed to study the LV and ESR models can be used to provide some new insights into the dynamical behavior of pioneer-climax models. This is something that we plan to investigate in the very near future.

Finally, we hope to locate some suitable experimental field data to use to make comparisons with the predictions obtained from LV, ESR and related discrete dynamical models in order to further demonstrate the usefulness of our work. It is in this endeavor that collaboration with one or more experts in the field of population biology would be very helpful.

APPENDIX A

DERIVATION OF THE PAIR OF INVERSE POINTS

In Section 2.6, in order to find the equation that will allow us to solve for the four possible inverse points, $F^{-1}(x, y)$, of $F(x_1, y_1)$ with any given point (x_1, y_1), we set

$$x_1 = \lambda x(1 - ax - by) \tag{A.1}$$

and

$$y_1 = \mu y(1 - cx - dy). \tag{A.2}$$

Then, from $(A.1)$, we get

$$\frac{x_1}{\lambda} = x - ax^2 - bxy, \tag{A.3}$$

and from $(A.2)$, we get

$$x = \frac{1}{c}\left(1 - dy - \frac{y_1}{\mu y}\right). \tag{A.4}$$

Now, we will solve for $y = y(a, b, c, d, \lambda, \mu, x_1, y_1)$ by substituting $(A.4)$ into $(A.3)$ and then $x = x(c, d, \mu, y_1, y)$. First, we obtain an equation

$$\begin{aligned} & c_4y^4 + c_3y^3 + c_2y^2 + c_1y + c_0 = 0 \quad \text{where} \\ c_4 &= d\mu^2(bc - ad), \\ c_3 &= \mu^2(2ad - bc - cd), \\ c_2 &= \mu^2(c - a - \tfrac{c^2x_1}{\lambda}) + \mu y_1(bc - 2ad), \\ c_1 &= \mu y_1(2a - c) \quad \text{and} \\ c_0 &= -ay_1^2. \end{aligned} \tag{A.5}$$

By using the Matlab command, $roots([c_4 \;\; c_3 \;\; c_2 \;\; c_1 \;\; c_0])$, we obtain four possible inverse values for y. We choose one of the four branches of $F^{-1}(x, y)$ that overlaps the original region. Then, we can subsequently solve for the corresponding x values to get our pair of inverse points by simply substituting the two y values of this branch into $(A.4)$.

APPENDIX B

LOCATION OF THE INTERSECTION POINT IN FIGURE 2.3

In Section 2.6, we observe in Figure 2.3 that there exists an intersection point of the parabolas $F(e_l)$ and $F(e_r)$. Here, we have

$$\begin{aligned} x_l &:= \tfrac{\lambda-1}{\lambda} - a \\ &\text{and} \\ x_r &:= \tfrac{\lambda-1}{\lambda} + b, \end{aligned} \tag{B.1}$$

and we want to solve the system of two equations

$$\begin{aligned} x_{int} &:= \lambda x_l(1 - x_l - \alpha y_{int}) \\ &\text{and} \\ x_{int} &:= \lambda x_r(1 - x_r - \alpha y_{int}) \end{aligned} \tag{B.2}$$

with two unknowns, x_{int} and y_{int}. So, by solving the equation

$$\lambda x_l(1 - x_l - \alpha y_{int}) = \lambda x_r(1 - x_r - \alpha y_{int}), \tag{B.3}$$

we obtain

$$y_{int} := \frac{1}{\alpha}(1 - x_l - x_r). \tag{B.4}$$

Therefore,

$$x_{int} := \lambda x_l x_r. \tag{B.5}$$

REFERENCES

1. K. Alligood, T. Sauer and J. Yorke, *Chaos: An Introduction to Dynamical Systems*, Springer-Verlag, New York, 1997.

2. L. Block, J. Guckenheimer, M. Misiurewicz and L. S. Young, Periodic points and topological entropy of one-dimensional maps, in *Global Theory of Dynamical Systems*, eds. Z. Nitecki and C. Robinson, Lect. Notes in Math., vol.811, pp.18–34, Springer-Verlag, New York, 1980.

3. P. Collet and J. Eckmann, *Iterated Maps on the Interval as Dynamical Systems*, Birkhäuser, Boston, 1980.

4. P. Cvitanovic, *Universality in Chaos*, Adam Hilger, 1984.

5. R. Devaney, *An Introduction to Chaotic Dynamical Systems*, 2nd ed., Addison-Wesley, Redwood City, 1989.

6. M. Feigenbaum, Quantitative universality for a class of nonlinear transformations, *J. Stat. Phys.*, 19 (1978), pp.25–52.

7. M. Gilpin, Spiral chaos in a predator-prey model, *Amer. Natur.*, 133 (1979), pp.306–308.

8. J. Guckenheimer and P. Holmes, *Nonlinear Oscillations, Dynamical Systems, and Bifurcations of Vector Fields*, Springer-Verlag, New York, 1983.

9. J. Guckenheimer, G. Oster and A. Ipatchi, The dynamics of density dependent population models, *J. Math. Biol.*, 4 (1977), pp.101–147.

10. A. Holden, ed., *Chaos*, Princeton University Press, Princeton, 1986.

11. O. Lanford, A computer-assisted proof of the Feigenbaum conjecture, *Bull. Amer. Math. Soc.*, 6 (1982), pp.427–434.

12. A. Lotka, *Elements of Mathematical Biology*, Dover, New York, 1956.

13. R. May, Simple mathematical models with very complicated dynamics, *Nature*, 261 (1976), pp.459–467.

14. R. May, Chaos and dynamics of biological populations, in *Dynamical Chaos*, eds. M. Berry, I. Percival and N. Weiss, pp.27–44, Princeton University Press, Princeton, 1987.

15. J. Milnor and W. Thurston, On iterated maps of the interval, in *Dynamical Systems*, College Park, 1986–87, Lect. Notes in Math., vol.1342, pp.465–563, Springer-Verlag, New York, 1988.

16. M. Shub, *Global Stability of Dynamical Systems*, Springer-Verlag, New York, 1987.

17. S. Smale, *The Mathematics of Time*, Springer-Verlag, New York, 1980.

18. V. Volterra, *Opere Matematiche: memorie e note*, Acc. Naz. dei Lincei, Roma, Cremona, Vol.V, pp.1–106, 1962.

19. D.K. Arrowsmith and C.M. Place, *Dynamical Systems: Differential equations, maps and chaotic behaviour*, Chapman and Hall, London, 1992.

20. Michael V. Berry, I.C. Percival and N.O. Weiss, *Dynamical Chaos*, Proceedings of the Royal Society of London, London, 1987.

21. Miklos Farkas, *Periodic Motions*, Springer-Verlag, New York, 1994.

22. H.I. Freedman, *Deterministic Mathematical Models in Population Ecology*, Marcel Dekker, Inc., New York, 1980.

23. M. Goossens, F. Mittelbach and A. Samarin, *The LaTeXCompanion*, Addison-Wesley, New York, 1994.

24. David F. Griffiths and Desmond J. Higham, *Learning LaTeX*, SIAM, Philadelphia, 1997.

25. John Guckenheimer, Jürgen Moser and Sheldon E. Newhouse, *Dynamical Systems*, Birkhauser, Boston, 1980.

26. J. Hale and H. Kocak, *Dynamics and Bifurcations*, Springer-Verlag, New York, 1991.

27. Nicholas J. Higham, *Handbook of Writing for the Mathematical Sciences*, SIAM, Philadelphia, 1998.

28. Richard A. Holmgren, *A First Course in Discrete Dynamical Systems*, Springer-Verlag, New York, 1996.

29. Yu. Ilyashenko and Weigu Li, *Nonlocal Bifurcations*, American Mathematical Society, Providence, 1999.

30. G. Lindfield and J. Penny, *Numerical Methods Using Matlab*, Ellis Horwood, New York, 1995.

31. Edward Lorenz, *The Essence of Chaos*, University of Washington Press, Seattle, 1993.

32. Mario Martelli, *Discrete Dynamical Systems and Chaos*, Longman Scientific and Technical, England, 1992.

33. Francis C. Moon, *Chaotic and Fractal Dynamics*, John Wiley and Sons, Inc., New York, 1992.

34. J.D. Murray, *Mathematical Biology*, Springer-Verlag, New York, 1993.

35. Tobias Oetiker, Hubert Partl, Irene Hyna and Elisabeth Schlegl, *The Not So Short Introduction to LaTeX2e*, Version 3.16, 25 September 2000.

36. Edward Ott, *Chaos in Dynamical Systems*, Cambridge University Press, Cambridge, 1993.

37. Lawrence Perko, *Differential Equations and Dynamical Systems*, Springer-Verlag, New York, 1991.

38. Clark Robinson, *Dynamical Systems: Stability, Symbolic Dynamics, and Chaos*, CRC Press, Inc., Boca Raton, 1995.

39. David Ruelle, *Chaotic Evolution and Strange Attractors*, Cambridge University Press, Cambridge, 1989.

40. Steven H. Strogatz, *Nonlinear Dynamics and Chaos*, Addison-Wesley, New York, 1994.

41. Fredinand Verhulst, *Nonlinear Differential Equations and Dynamical Systems*, Springer-Verlag, New York, 1996.

42. S. Wiggins, *Global Bifurcations and Chaos*, Springer-Verlag, New York, 1988.

43. S. Wiggins, *Introduction to Applied Nonlinear Dynamical Systems and Chaos*, Springer-Verlag, New York, 1990.

44. D. Blackmore, J. Chen, J. Perez and M. Savescu, Dynamical properties of discrete Lotka-Volterra equations, *Chaos, Solitons and Fractals*, accepted for publication, September 2000.

45. Chai-wei Chi, Sze-bi Hsu and Lih-ing Wu, On the asymmetric May-Leonard model of three competing species, *SIAM Journal of Applied Mathematics*, Vol.58 No.1 (1998), pp.211–226.

46. F.C. Hoppensteadt, *Mathematical Models of Population Biology*, Courant Institute of Mathematical Sciences, New York, 1976.

47. Robert Rosen, *Dynamical System Theory in Biology*, Vol.1, Wiley-Interscience, New York, 1970.

48. Paul Waltman, *Competition Models in Population Biology*, CBMS 45, SIAM, Philadelphia, 1983.

49. R.M. Nisbet and L.C. Onyiah, Population dynamic consequences of competition within and between age classes, *J. Math. Biol.* 32 (1994), pp.329–344.

50. R.F. Costantino, J.M. Cushing, B. Dennis and R.A. Desharnais, Exponentially induced transitions in the dynamic behavior of insect populations, *Nature* 375 (1995), pp.227–230.

51. S. Smale, Diffeomorphisms with many periodic points, In *Differential and Combinatorial Topology*, S.S. Cairns (ed.), pp.63–80, Princeton University Press, Princeton, 1963.

52. Simon A. Levin, Mathematical population biology, *Proceedings of Symposia in Applied Mathematics*, Vol.30 (1984), pp.1–8.

53. R.M. May, *Stability and Complexity in Model Ecosystems*, Princeton University Press, Princeton, 1974.

54. R.M. May, Mathematical aspects of the dynamics of animal populations, *Populations and Communities*, MAA, Washington, 1978.

55. T.Y. Li and J. Yorke, Period three implies chaos, *Amer. Math. Monthly*, Vol.82 (1975), pp.985–992.

56. D.K. Arrowsmith and C.M. Place, *An Introduction to Dynamical Systems*, Cambridge University Press, Cambridge, 1990.

57. J. Franke and A. Yakubu, Geometry of exclusion principles in discrete systems, *J. Math. Anal. Appl.* 168 No.2 (1992), pp.385–400.

58. J. Franke and A. Yakubu, Global attractors in competitive systems, *Nonlin. Anal. Theory Meth. Appl.* 16 (1991), pp.111–129.

59. J. Franke and A. Yakubu, Mutual exclusion versus coexistence for discrete competitive systems, *J. Math. Biol.* 30 (1991), pp.161–168.

60. J. Franke and A. Yakubu, Extinction and persistence of species in discrete competitive systems with a safe refuge, *J. Math. Anal. Appl.* 203 No.3 (1996), pp.746–761.

61. G. Namkoong and J. Selgrade, Stable periodic behavior in a pioneer-climax model, *Nat. Res. Model.* 4 (1990), pp.215–227.